AD-A261 248

MENTATION PAGE

Form Approved
OMB No. 0704-0188

(2)

REPORT DATE	3. REPORT TYPE AND DATES COVERED
	Reprint 1 May-1 November 1992

4. TITLE AND SUBTITLE

NCSU Electrothermal Launcher "SIRENS" Research Program

5. FUNDING NUMBERS

DAAL03-92-G-0051

6. AUTHOR(S)

M. Bourham, J. Gilligan and O. Hankins

7. PERFORMING ORGANIZATION NAME(S) AND ADDRESS(ES)

North Carolina State University
Department of Nuclear Engineering
Raleigh, NC 27695-7909

8. PERFORMING ORGANIZATION REPORT NUMBER

9. SPONSORING/MONITORING AGENCY NAME(S) AND ADDRESS(ES)

U. S. Army Research Office
P. O. Box 12211
Research Triangle Park, NC 27709-2211

10. SPONSORING/MONITORING AGENCY REPORT NUMBER

ARO 30258.3-RT-AAS

11. SUPPLEMENTARY NOTES

The view, opinions and/or findings contained in this report are those of the author(s) and should not be construed as an official Department of the Army position, policy, or decision, unless so designated by other documentation.

12a. DISTRIBUTION/AVAILABILITY STATEMENT

Approved for public release; distribution unlimited.

12b. DISTRIBUTION CODE

13. ABSTRACT *(Maximum 200 words)*

A review of SIRENS electrothermal launcher research program is presented. SIRENS research program focuses on the understanding of boundary layer physics with typical EM/ET plasma characteristics. Diagnostics development includes in-bore measurements of high heat flux and plasma conductivity. A comparison between the erosion of various material surfaces under typical EM/ET high heat loading conditions is also presented. Fuseless (vacuum) versus fuse (atmospheric) operation showed that barrel pressure may reach 0.75 kbar at an input energy of 5 kJ to the source.

14. SUBJECT TERMS	15. NUMBER OF PAGES
Materials erosion, boundary layer physics, ablation and viscous drags, vapor shield, magnetic vapor shield.	16. PRICE CODE

17. SECURITY CLASSIFICATION OF REPORT	18. SECURITY CLASSIFICATION OF THIS PAGE	19. SECURITY CLASSIFICATION OF ABSTRACT	20. LIMITATION OF ABSTRACT
UNCLASSIFIED	UNCLASSIFIED	UNCLASSIFIED	UL

PRESENTED AT THE 10TH ELECTROMAGNETIC
LAUNCHER ASSOCIATION MEETING (10th),
DAYTON, OHIO, SEPTEMBER 15-17, 1992.

NCSU ELECTROTHERMAL LAUNCHER "SIRENS" RESEARCH PROGRAM

MOHAMED BOURHAM, JOHN GILLIGAN, ORLANDO HANKINS
Department of Nuclear Engineering, North Carolina State University
Raleigh, NC 27695-7909

Key words: Materials Erosion, Boundary Layer Physics, Ablation and Viscous Drags, Vapor Shield, Magnetic Vapor Shield

Work supported by the US Army Strategic Defense Command Contract DASG60-90-C-0028, US Army Watervliet Arsenal Contract DAAA22-91-M-4001, and US Army Research Office Contract DAAL03-92-G-0051.

10th Electromagnetic Launcher Association Meeting
Dayton, Ohio, September 15-17, 1992

NCSU ELECTROTHERMAL LAUNCHER "SIRENS" RESEARCH PROGRAM

Mohamed Bourham, John Gilligan, Orlando Hankins
Department of Nuclear Engineering, North Carolina State University
Raleigh, NC 27695-7909

Key words: Materials Erosion, Boundary Layer Physics, Ablation and Viscous Drag, Vapor Shield, Magnetic Vapor Shield.

Work supported by the US Army Strategic Defense Command Contract DASG60-90-C-0028, US Army Watervliet Arsenal Contract DAAA22-91-M-4001, US Army Research Office Contract DAL03-92-G-0051.

Objectives of the Project

- To understand and control the basic energy transport phenomena in the Vapor Shield at different material surfaces under high heat flux.
- To explore the effect of a strong magnetic field in decreasing surface erosion and drag coefficients under high heat flux under EM gun conditions.
- To model the Magnetic Vapor Shield mechanism and to compare with experimental results.
- To understand, characterize, and control the plasma-propellant energy transport process by measuring propellant burn rates.
- To explore and model the plasma-propellant interaction process and the flame vapor shield mechanism.
- To systematically diagnose and explore the reaction of different propellants under different injected plasma conditions.

Major Issues to Investigate

- To systematically explore the resistance of various materials (insulators, composites, metals and alloys, non-metallic conductors, metallic and diamond coatings, etc.) to high heat flux erosion, and plasma reactions with solid and liquid propellants.
- To determine the nature of drag forces and turbulent convective flow in contributing to surface erosion.
- To fully diagnose the vapor shield plasma, and the plasma and heat flux distribution onto propellant samples.
- To model and predict the vapor shield effectiveness both with and without a magnetic field, and model and predict the flame vapor shield effect and burn rate of propellants.

Accomplishments

1989/1990

- Predicted vapor shield transmission factors that were verified by experiment. Energy transmission factor through the vapor shield is on the order of 10%. Radiation transport is the most important energy transfer mechanism. Demonstrated that some materials have better vapor shielding properties than others.

- Erosion of different materials was explored, and the axial erosion dependence was measured for different materials. SEM, EDXA and Auger analyses demonstrate the redeposition of electrode materials at different locations. Conditioning effects of single material samples exposed to multiple shots were noted, which will be important in operation of railguns.

- The spectra of observed plasma light emission indicated the presence of electrode and sample materials.

- Preliminary results on the effect of the magnetic field. Magnetic fields decreased surface erosion by 20% for fields of 5 Tesla.

- Developed series of 1-D, time-dependent, MHD codes to model vapor shield phenomena, ZEUS, a global, time dependent code for the source plasma, and MAGFIRE, a 1-D, time dependent MHD code with coupled radiation transport for ablative plasma.

1990/1991

- Generated materials erosion data base for metals, alloys, insulators, non-metallic conductors and refractory materials. Demonstrated that metallic surfaces have mixed melting/erosion with strong axial erosion dependence, while insulators and graphites ablate homogeneously along the axis.

- Modified the chamber geometry (10 inch cross connected to the 6 inch cross).

- Modified diagnostics arrangements and developed in-bore heat flux (direct and indirect measurement of heat flux to the wall) with 1-D and 2-D, time dependent heat flux codes "SURFHEAT and 2DSURFHEAT", and plasma conductivity diagnostic technique.

- Obtained empirical general scaling law of the energy transmission factor f through the vapor shield layer (for different materials) for ideal and non-ideal plasma models, $f = K_1 + K_2 S^{-1/4}$, where K_1 and K_2 are constants depending on material properties, S is the source fluence.

- Obtained results on the effect of the magnetic field (Magnetic Vapor Shield) with fields up to 8.75T. Magnetic fields decreased surface erosion by up to 35% for fields of 6.25 Tesla. An empirical general scaling law of the energy transmission factor for Lexan with the effect of the magnetic field, $f_{(S,B)}$ has been obtained, $f_{(S,B)} = \Phi_1(B)\ S^{-1/4} + \Phi_2(B)$, where $\Phi_1(B)$, $\Phi_2(B)$ are quadratic functions of the magnetic field.

1991/1992

- Identified species that appear in the majority of the discharges. C_2 (Swan bands), CH_4 (absorption line), neutral copper (from the electrodes), and neutral carbon.

- Measured the source average plasma temperature using optical emission spectroscopy, correlated to conductivity probes and heat flux measurements, and calculations based on the source ablation and ZEUS-code predictions.

- Continuous materials erosion studies on coated surfaces with different coating techniques, tungsten, tantalum and chromium alloys, ceramic insulators and diamond coatings.

- Modified SURFHEAT code to include melting. Plasma temperature deduced from heat flux measurements correlates well with values obtained from optical emission spectroscopy. The updated version of SURFHEAT yields more accurate results in heat flux diagnostics.

- Detailed analysis of the magnetic vapor shield, including convection heat flux, velocity slowdown, and photon attenuation within the boundary layer.

- Accelerating projectiles, 0.33 g Lexan projectiles, and velocity measurements using break wires, photo-interrupters, laser cut-off, and absolute pressure transducers "fuse-atmospheric and fuseless-vacuum operation".

- Drag forces measurements, using absolute pressure transducers inside a special diagnostics barrel. Measured 0.8 kbar pressure inside the barrel at 5 kJ input energy "fuse and fuseless operation".

SIRENS OPERATIONAL CHARACTERISTICS

DISCHARGE VOLTAGE (10 kV max.)	1 - 8 kV
PEAK CURRENT (100 kA max.)	20-100kA
NET INPUT ENERGY (15 kJ max.)	1 - 8 kJ
DISCHARGE PERIOD	100 μsec
RADIATED POWER	2-70 GW/m^2
PEAK PRESSURE	> 1 kbar
PLASMA DENSITY	10^{25}-$10^{26}m^{-3}$
PEAK PLASMA TEMPERATURE	4 - 6 eV
AVERAGE PLASMA TEMPERATURE	1 - 3 eV
AVERAGE PLASMA VELOCITY	≈12 km/sec

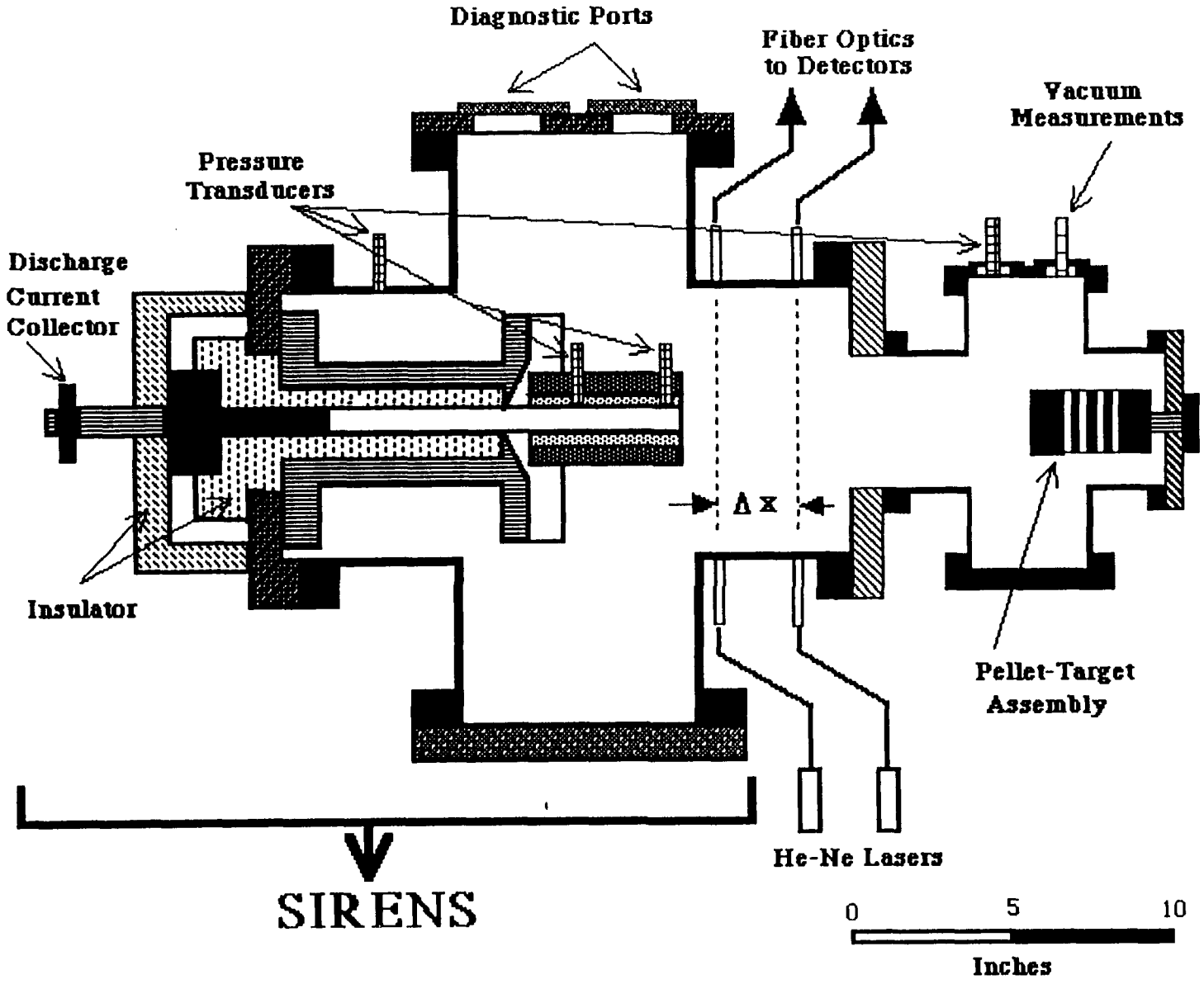

SIRENS "upgrade"

DIAGNOSTICS

PLASMA DIAGNOSTICS (UP TO 18 CHANNELS)

ROGOWSKI COILS => DISCHARGE CURRENT, PLASMA CURRENT, MAGNET CURRENT)

B-DOT LOOPS => B-DOT SIGNALS (WITHOUT BARREL, OR WITH SPECIAL BARREL)

COMPENSATED POTENTIAL DIVIDERS => DISCHARGE POTENTIAL

MAGNETIC PROBES => MAGNET B-FIELD

THERMOCOUPLES => HEAT FLUX

CONDUCTIVITY PROBES => PLASMA RESISTANCE

PRESSURE TRANSDUCERS => TIME-RESOLVED ABSOLUTE PRESSURE

He-Ne LASER, PHOTO-TRANSISTORS, OPTO-INTERRUPTERS, BREAK WIRES => VELOCITY

HEAT FLUX CALORIMETRY

OPTICAL MULTICHANNEL ANALYZER => TIME-INTEGRATED VISIBLE SPECTRUM

MONOCHROMATORS => TIME-RESOLVED SPECTRAL LINES

MATERIAL DIAGNOSTICS

MICROBALANCE => WEIGHT LOSS

SEM => SURFACE ANALYSIS

EDXA = > SURFACE ELEMENTAL ANALYSIS

AES => SURFACE ELEMENTAL ANALYSIS

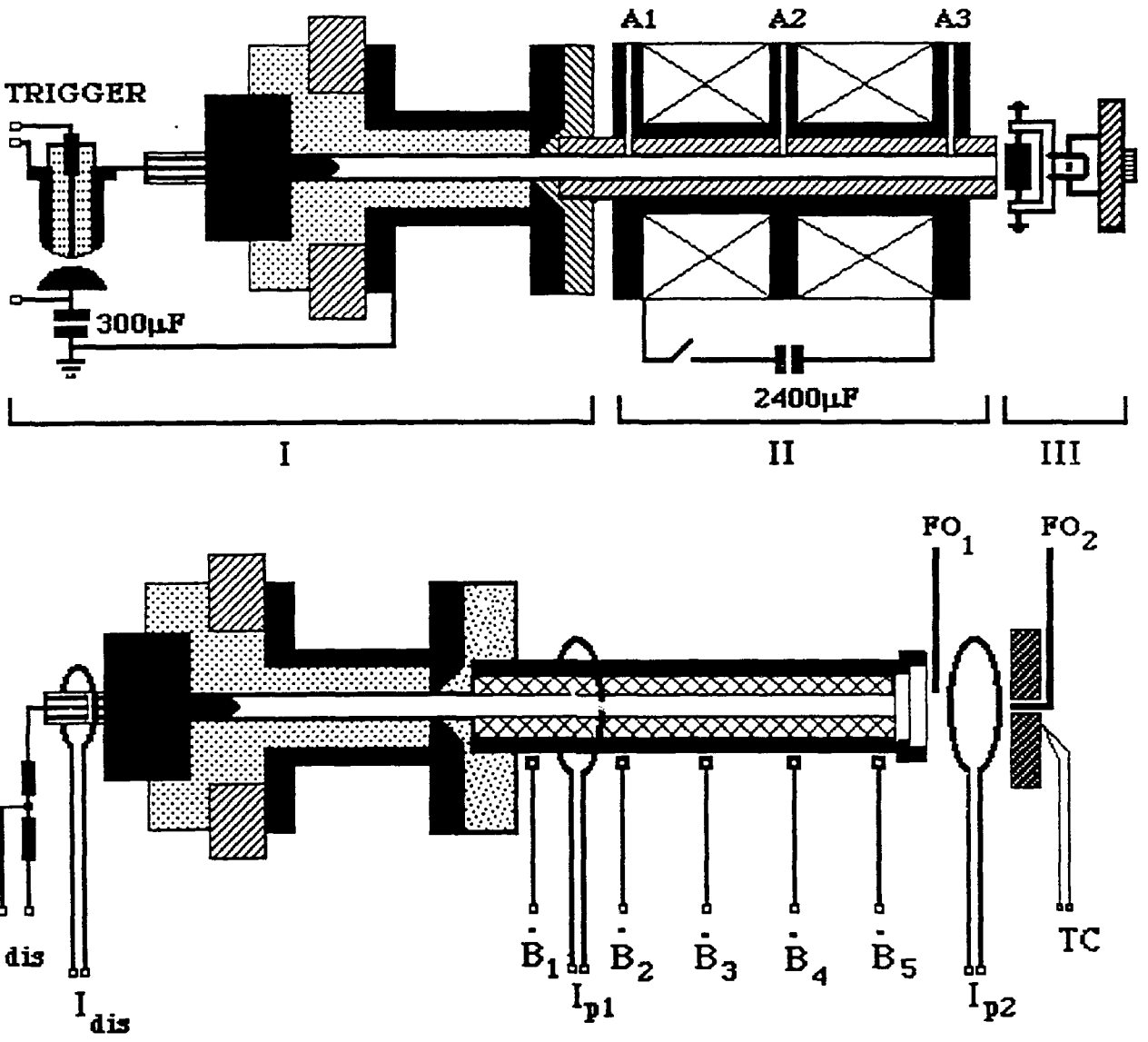

TOP: Schematic of SIRENS showing the source section (capillary), barrel section with magnet assembly (magnetic vapor shield studies).

BOTTOM: Diagnostics arrangement showing standard diagnostics (currents, voltage, B-dots), fiber optics for optical emission spectroscopy, and a thermocouple for heat flux measurements.

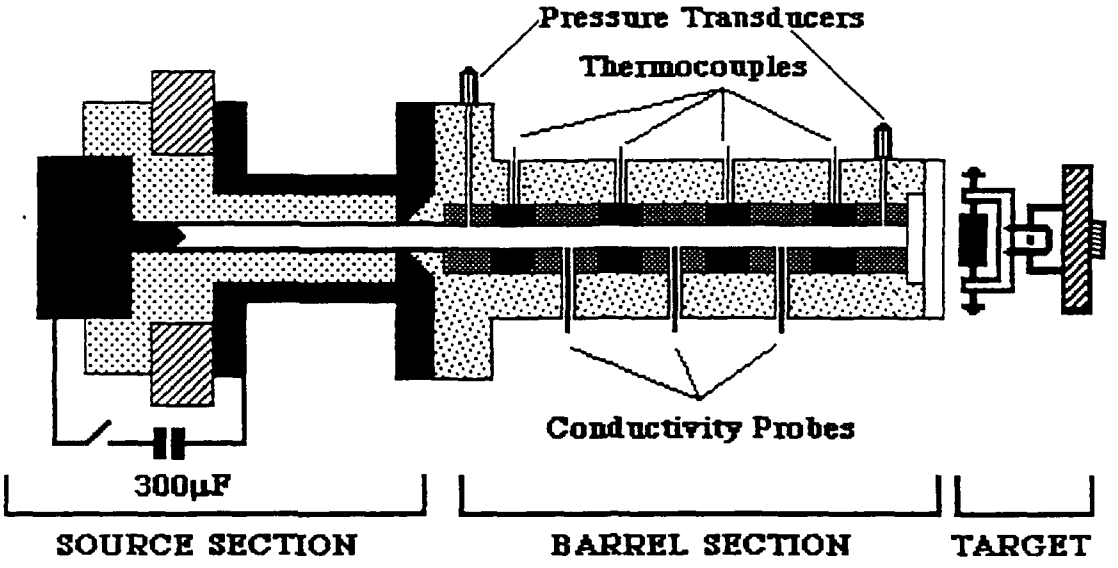

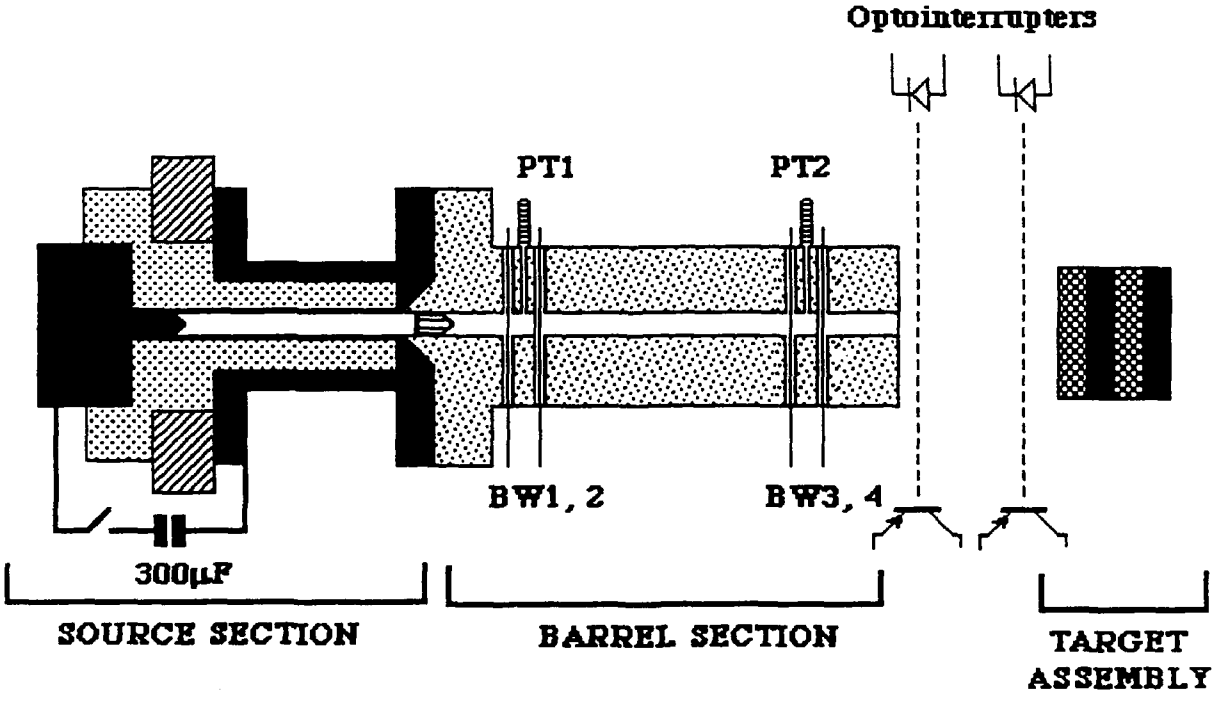

BARREL DIAGNOSTICS

TOP: conductivity probes (resistivity), thermocouples (heat flux), and pressure.

BOTTOM: Break wires (velocity), pressure (drags), and optointerrupters (velocity).

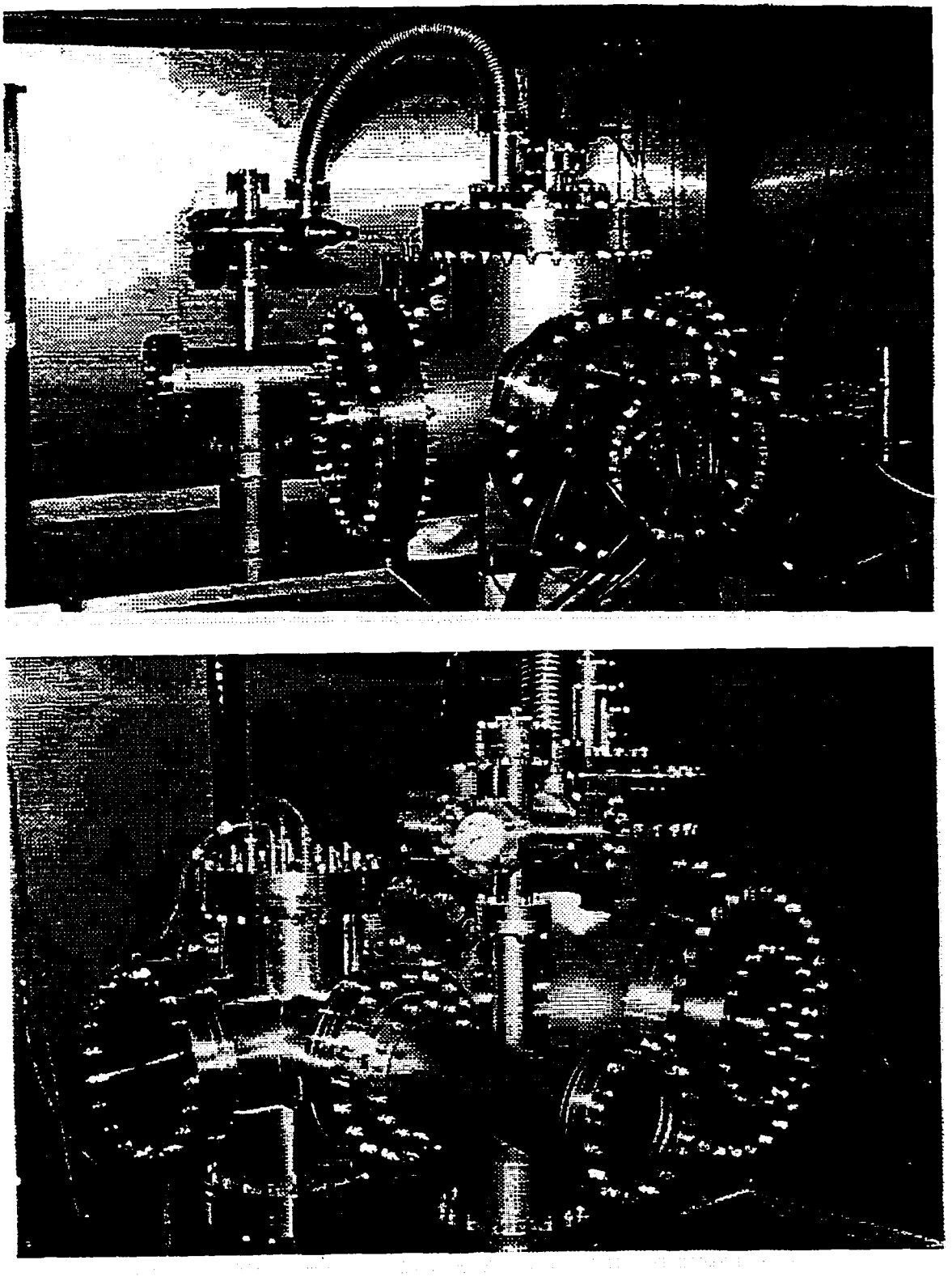

Photographs of SIRENS showing the source input section and magnet current feedthrough (top photo), and target and expansion chamber with diagnostics feedthrough (bottom photo).

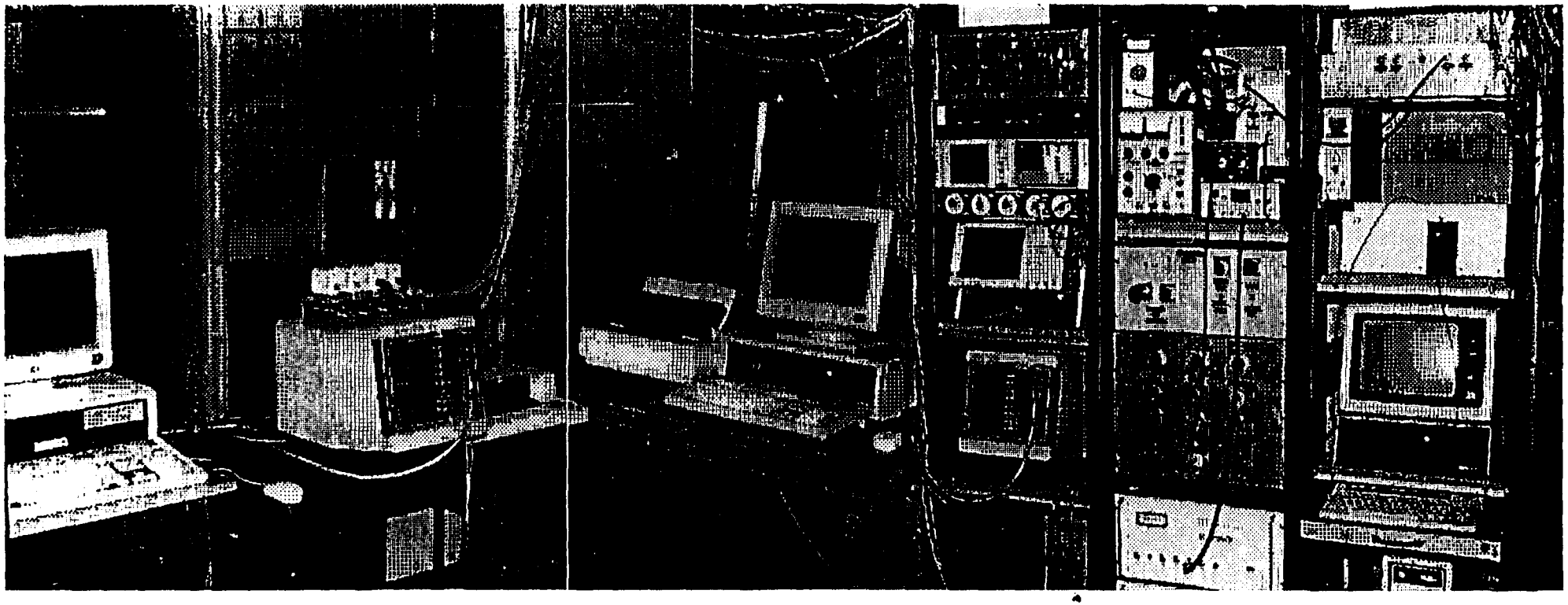

Waveform digitizer connected to 4 thermocouple modules for heat flux measurements. SURFHEAT reads the temperature data files and calculates the incident heat.

Waveform digitizer interfaced to several diagnostics (current, voltage, conductivity, etc.). Pump controls and modular potential divider are shown on the control panel.

Central rack shows power supplies and main controls.

Optical multichannel analyzer.

Photograph showing SIRENS diagnostics and control room

Shot # 362
Net Energy Input: 5.008 kJ
Material: Tantalum on Copper Substrate
(Ta sputtering on Cu substrate, 25 μ thick)
"RUN No. 125-4"

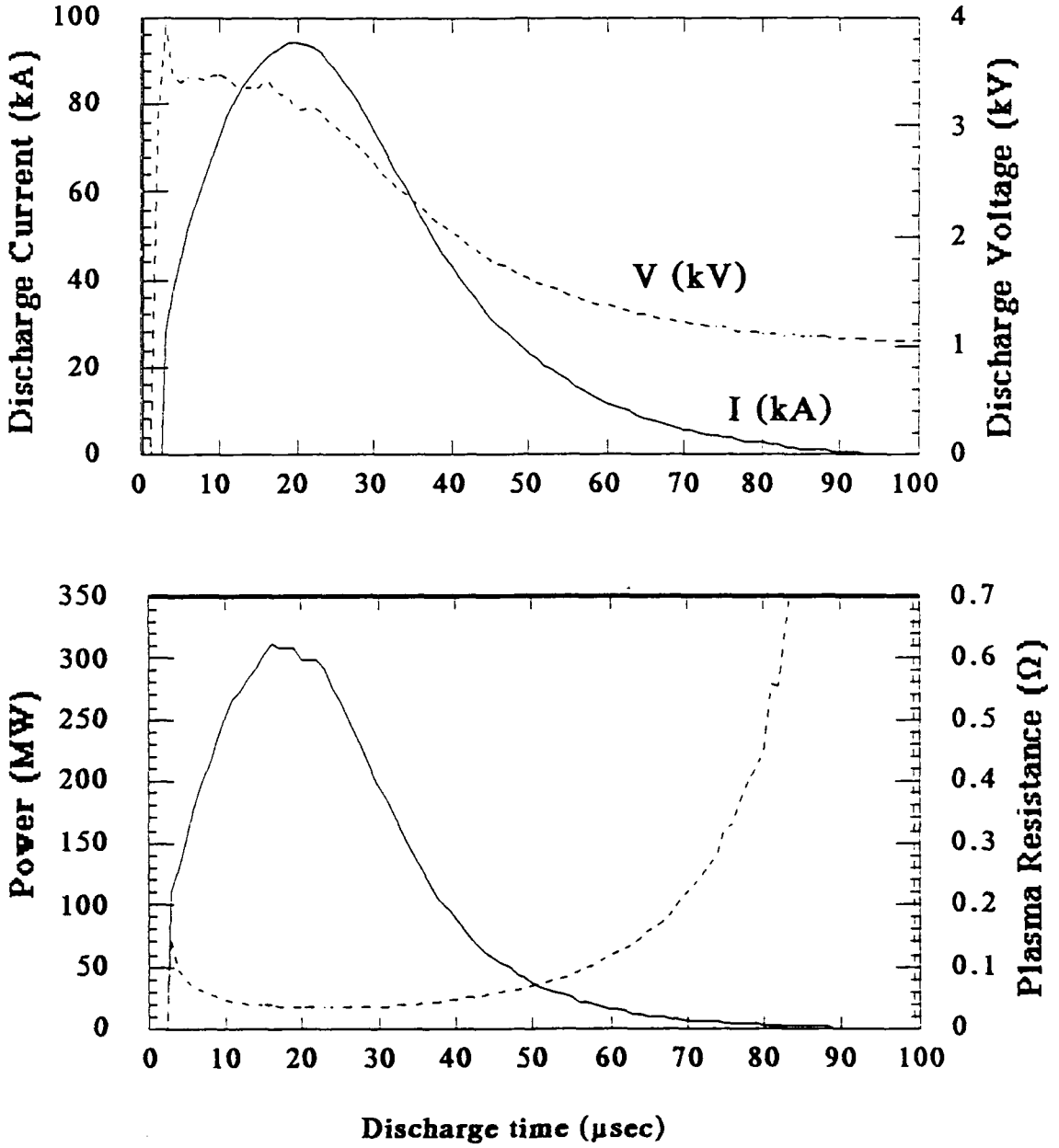

Oscillograms of discharge current and voltage (top), and calculated power and resistance (bottom).

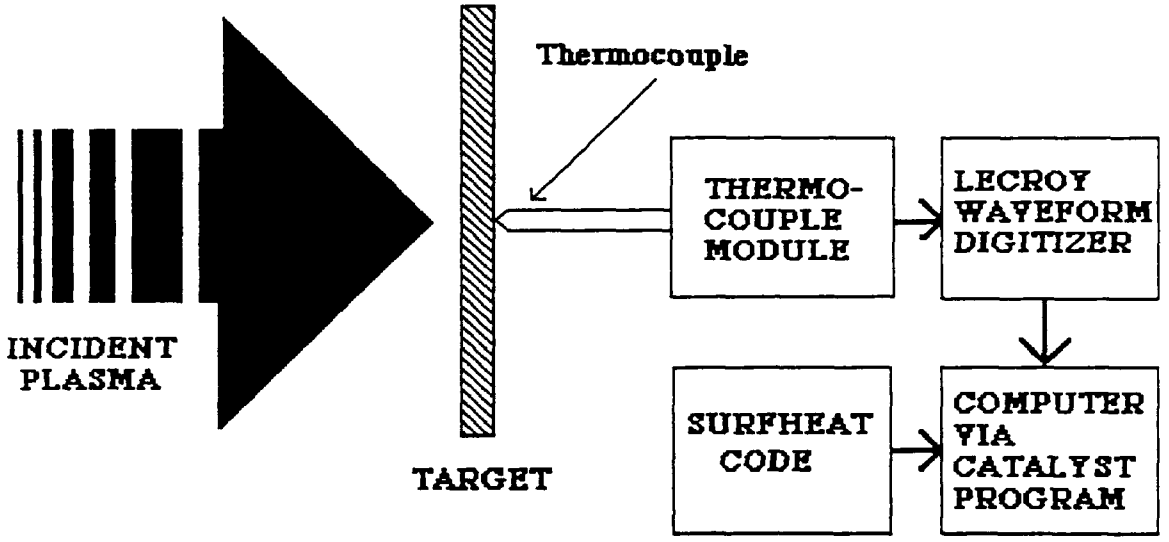

SCHEMATIC OF HEAT FLUX MEASUREMENTS

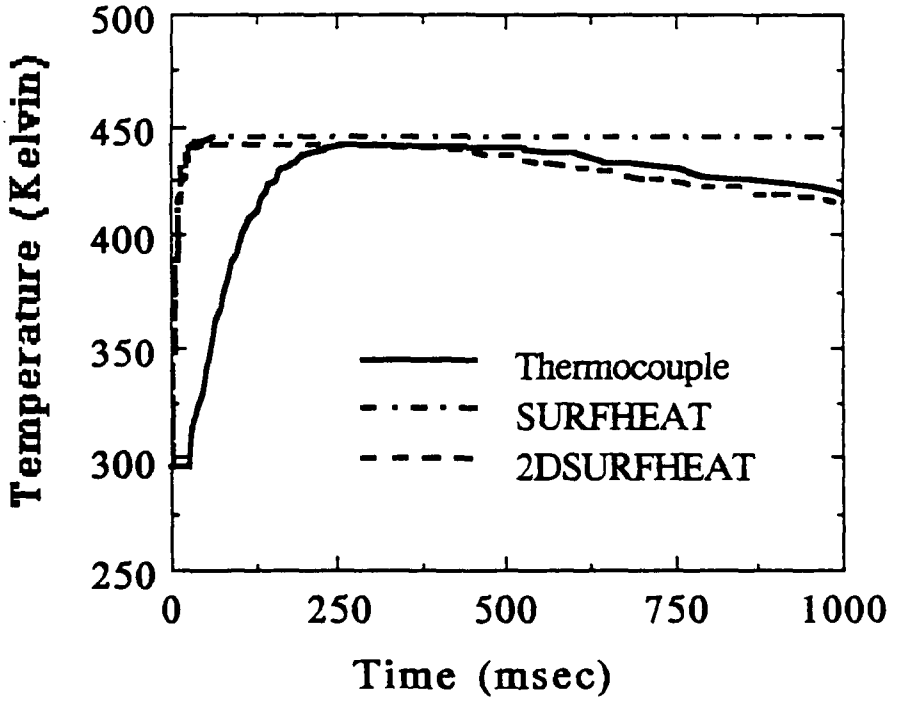

MEASURED AND CALCULATED TEMPERATURE HISTORIES

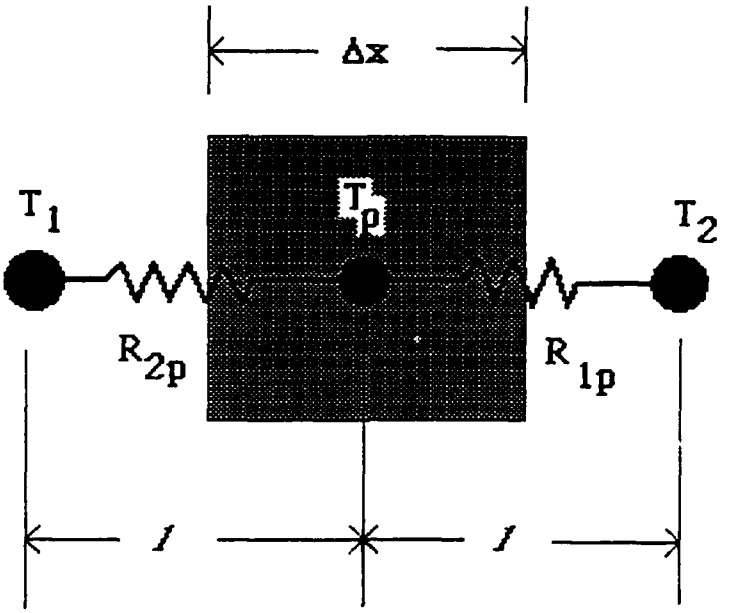

$$\sum_{j=1}^{2} \frac{T_j^i - T_p^i}{R_{jp}} + A_p\, q^{\cdot} = \rho\, C_p\, \Delta V \left[\frac{T_p^{i+1} - T_p^i}{\Delta t} \right]$$

with $R_{jp} = \left[\frac{\ell}{k A_j} \right]_{jp}$ = Thermal resistance between nodes j and p

Nodal equations:

Front surface: $$T_1^{i+1} = T_1^i + \frac{2\Delta t}{\rho\, C_p\, \Delta x^2} \left\{ k(T_2^i - T_1^i) + \Delta x\, q^{\cdot} \right\}$$

Interior region: $$T_m^{i+1} = T_m^i + \frac{\Delta t}{\rho\, C_p\, \Delta x^2} \left\{ k(T_{m-1}^i - T_m^i) + k(T_{m+1}^i - T_m^i) \right\}$$

Back surface: $$T_{n+1}^{i+1} = T_{n+1}^i + \frac{2\Delta t}{\rho\, C_p\, \Delta x^2} \left\{ k(T_{n+1}^i - T_n^i) + \Delta x\, q^{\cdot} \right\}$$

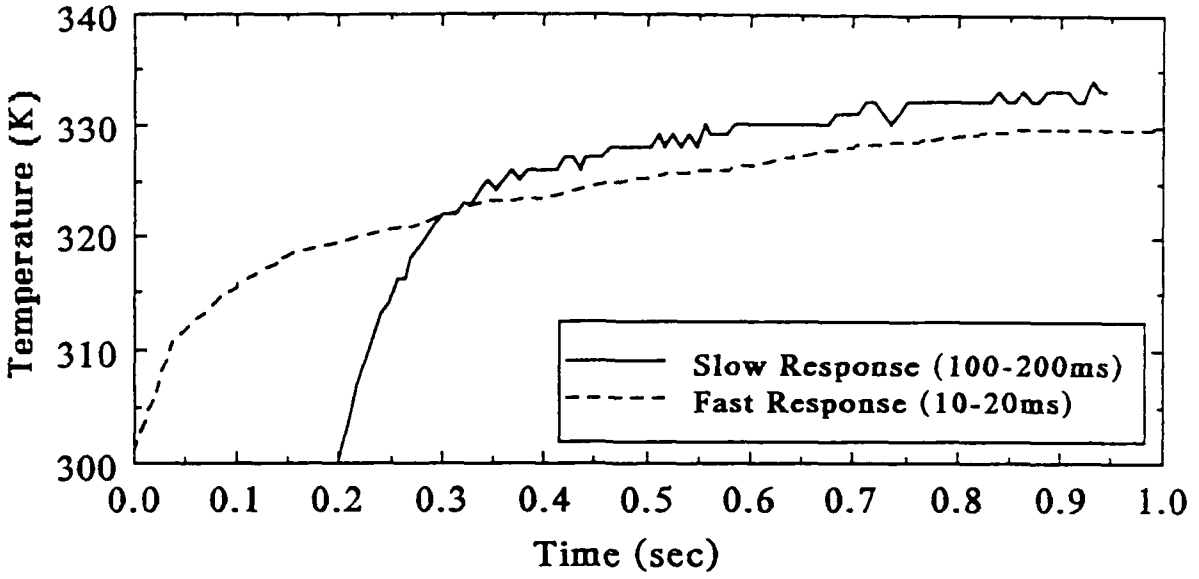

COMPARISON BETWEEN TEMPERATURE HISTORIES OBTAINED BY SLOW AND FAST RESPONSE THERMOCOUPLES

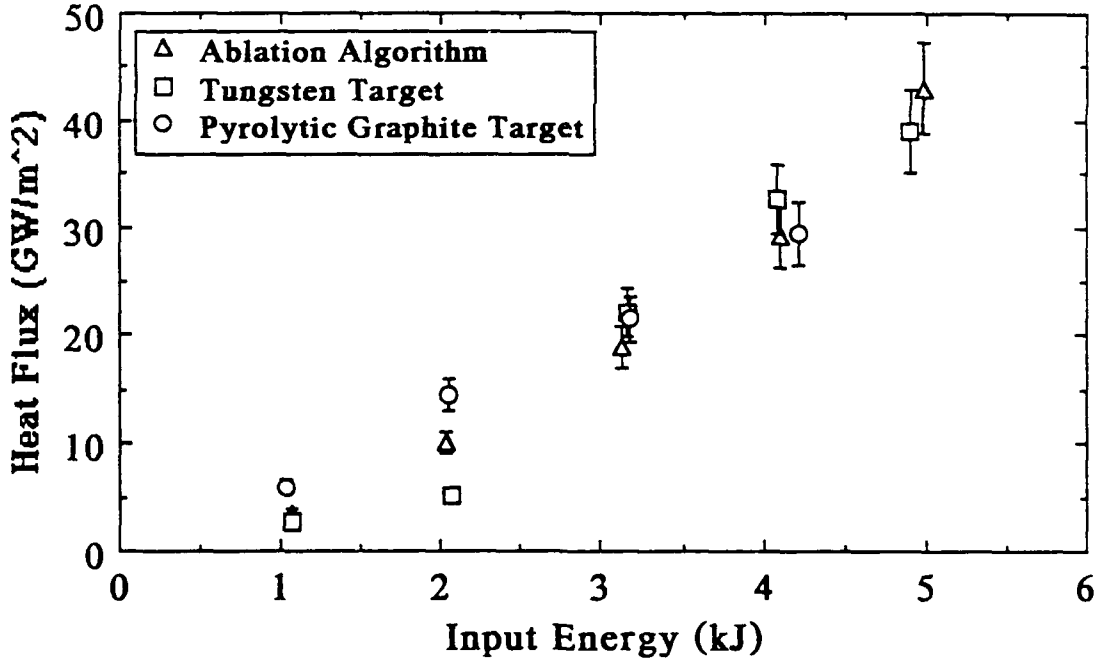

HEAT FLUX RESULTS FOR A TUNGSTEN ALLOY TARGET (MELT LAYER REMOVED) COMPARED TO PYROLYTIC GRAPHITE TARGET (ABLATION OF TARGET SURFACE), AND SOURCE ABLATION ALGORITHM.

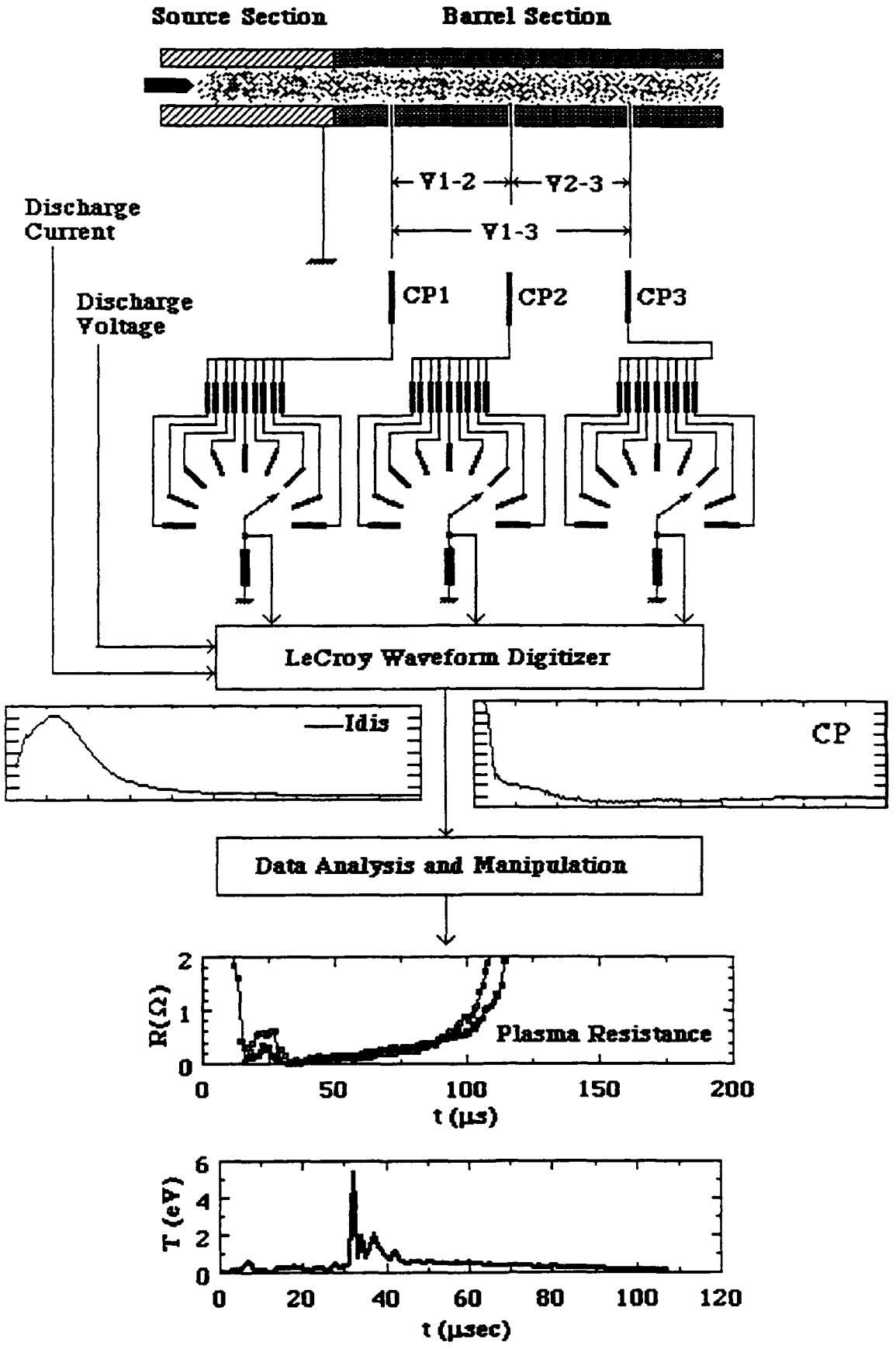

Conductivity probes are connected to a modular potential divider, where the potential between each two probes is recorded. Probe potentials, discharge current and voltage data are recorded with a LeCroy 6810 waveform digitizer interfaced to a PC via GPIB/PC-2. Through data analysis and manipulation, plasma resistivity (and consequently plasma temperature) can be extracted.

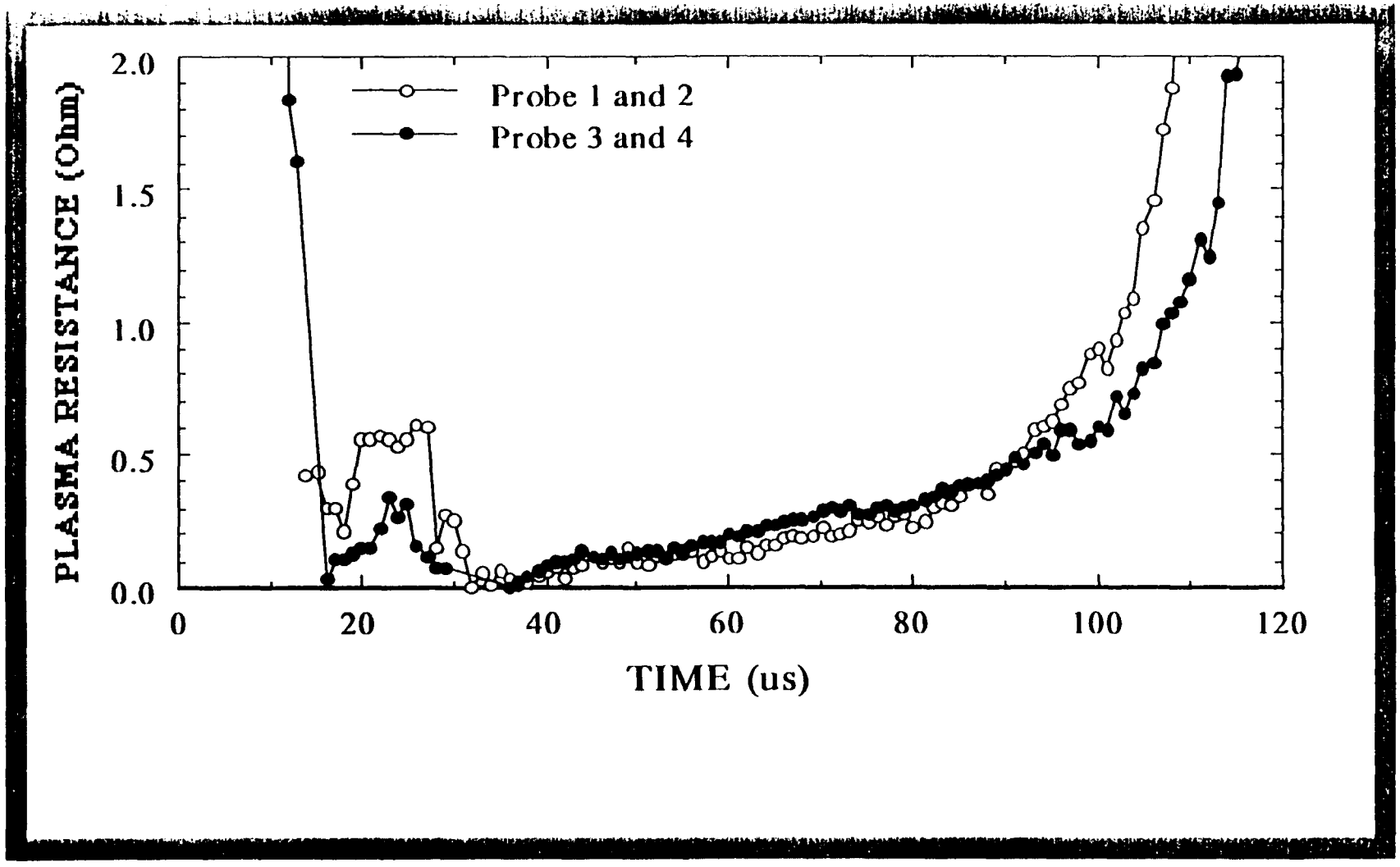

PLASMA RESISTANCE OBTAINED FROM CONDUCTIVITY PROBES ALONG THE BARREL AXIAL DIRECTION

The resistivity model for weakly nonideal plasmas is evaluated from:

$$\eta_{ei} = \eta_{ei0} \frac{\ln (1+1.4 \Lambda_m^2)^{1/2}}{\ln(\Lambda)} (\frac{\Omega}{\Omega - 1})$$

where, $\ln (1+1.4 \Lambda_m^2)^{1/2}$ replaces the Coulomb logarithm $\ln(\Lambda)$ to account for the nonideal effects, and $\Lambda m = (\Lambda r_S^*)$ where $r_S^* (= r_S/\lambda_D)$ is the normalized non-Debye screening radius; η_{ei0} is the Spitzer resistivity model, and Ω represents the term for the localization of electrons due to incomplete screening:

$$\Omega = (1 + 0.8 \frac{kT}{w})^4$$

where w is the energy dispersion due to electric microfields.

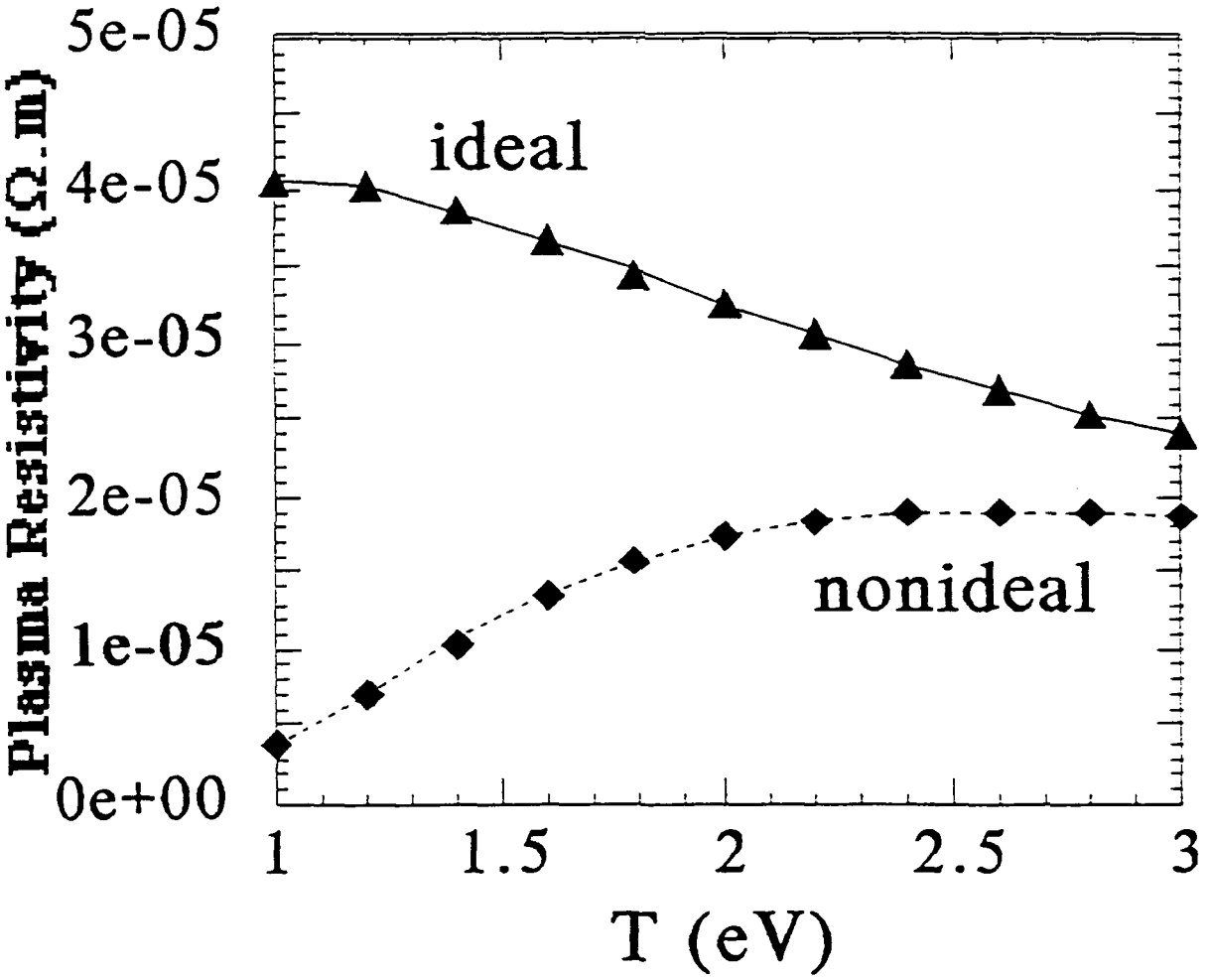

Ideal and nonideal plasma resistivities for a plasma density of $10^{26}/m^3$, and an average charge state = 1.0

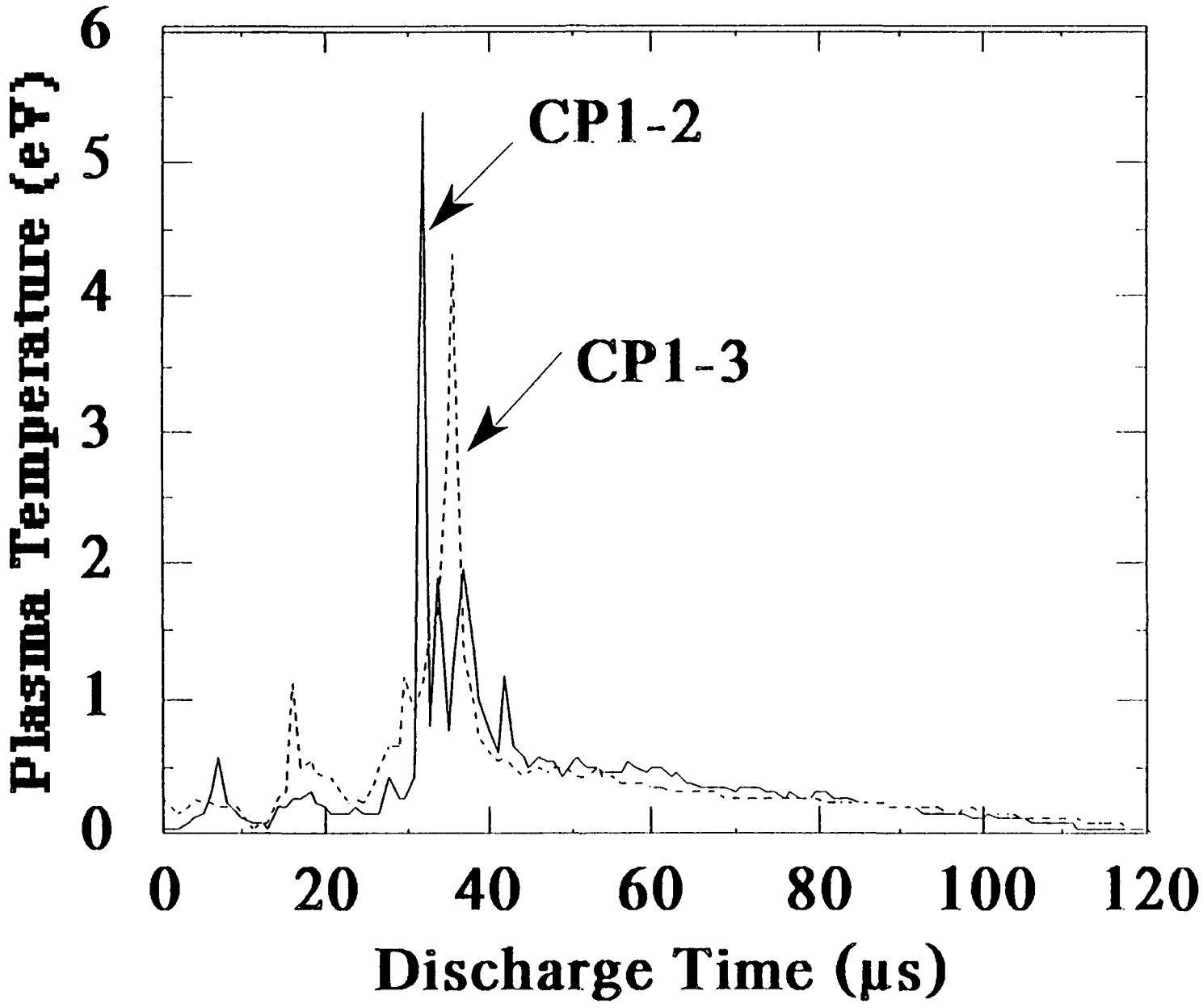

Plasma temperature as a function of the discharge time, calculated from conductivity probes (CP1-2 and CP1-3) and discharge current, for 1.17 kJ input energy.

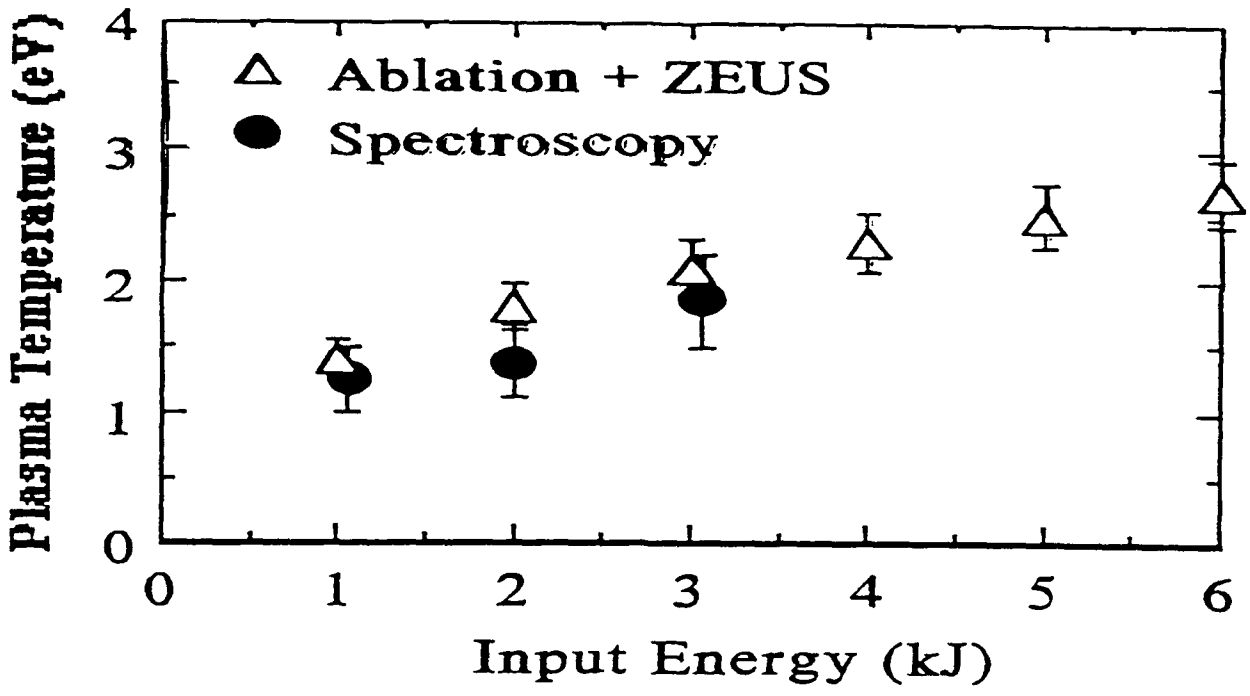

Temperatures of the source plasma deduced from ablation measurements and ZEUS code. Also shown are temperatures as calculated by Optical Emission Spectroscopy

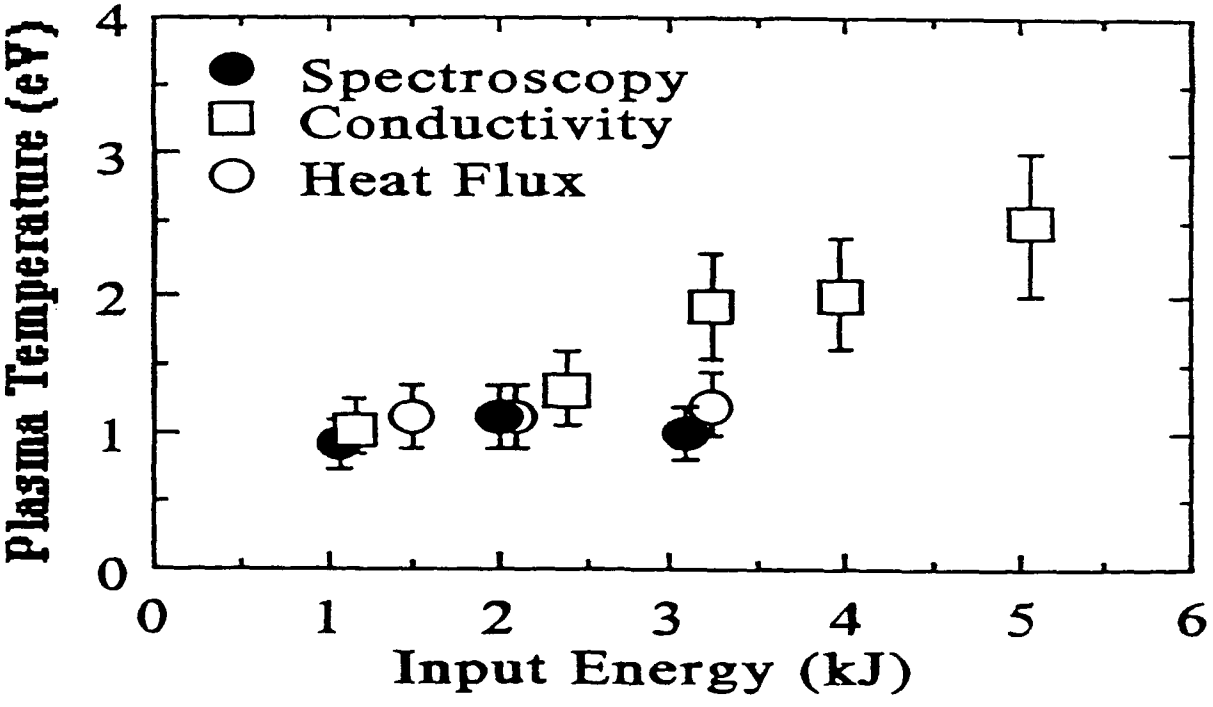

Average plasma temperatures in the barrel deduced from heat flux and conductivity measurements. Also shown temperatures as determined by Optical Emission Spectroscopy.

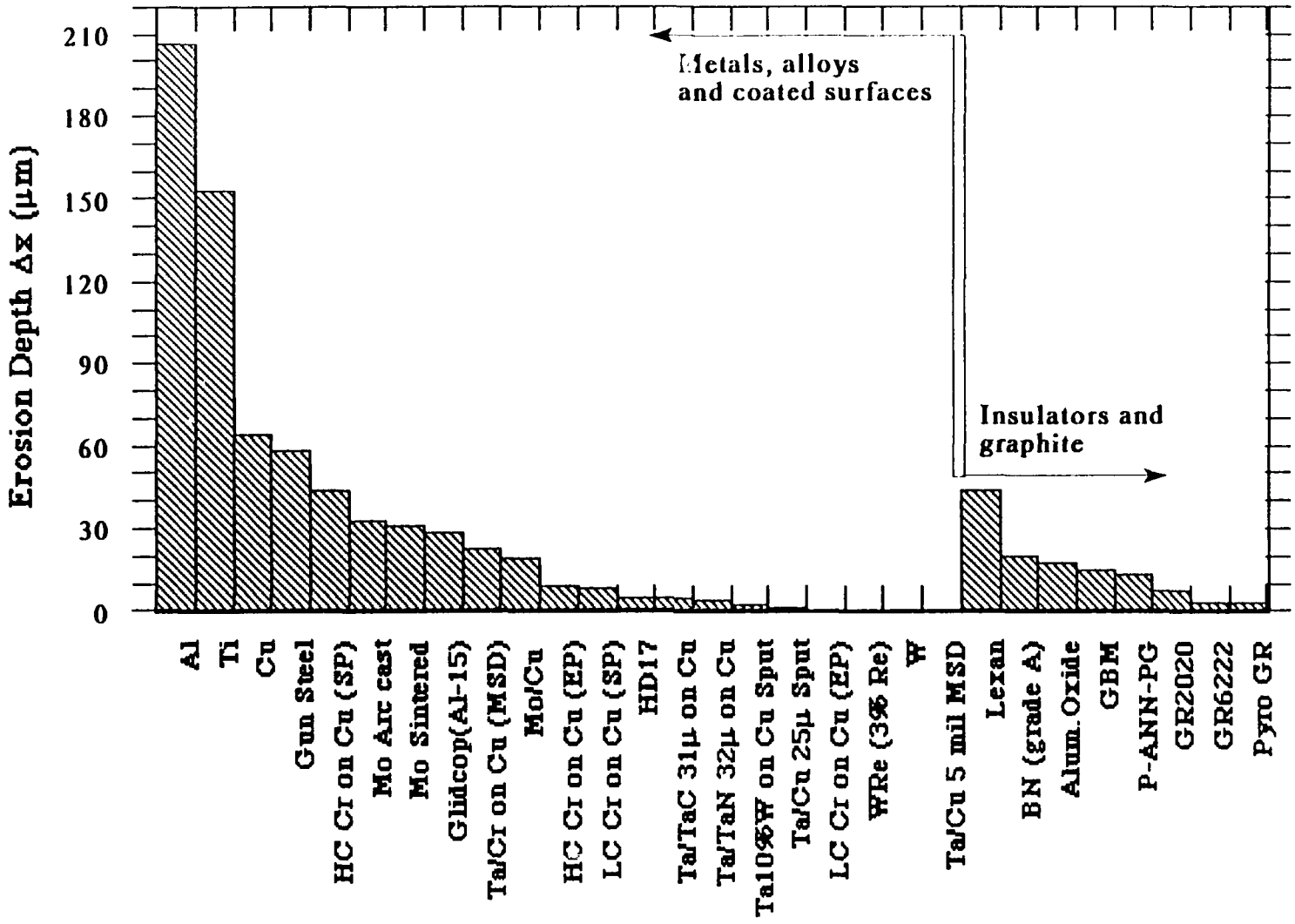

Comparison between measured erosion for pure metals, alloys, coated surfaces, insulators and graphite, at an incident heat flux of 33 GW/m^2 over 100 μs

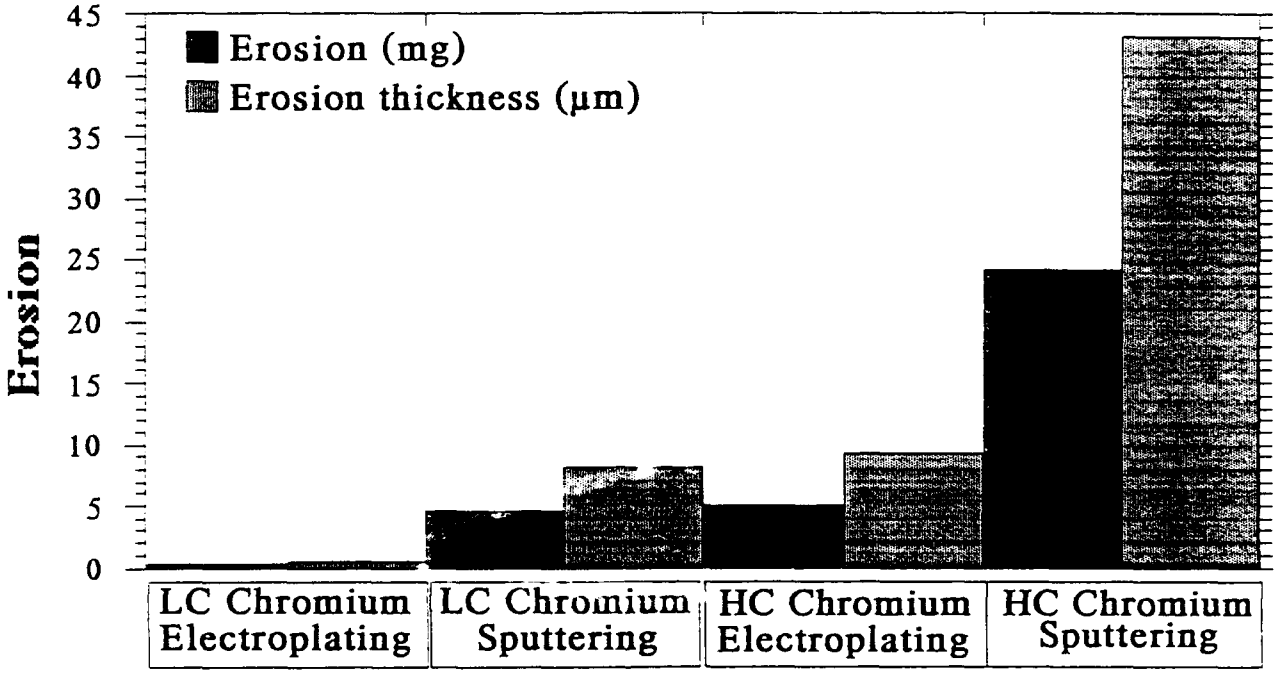

Comparison of L.C. and H.C. Chromium coatings on copper, for tested samples prepared via electroplating and sputter deposition.

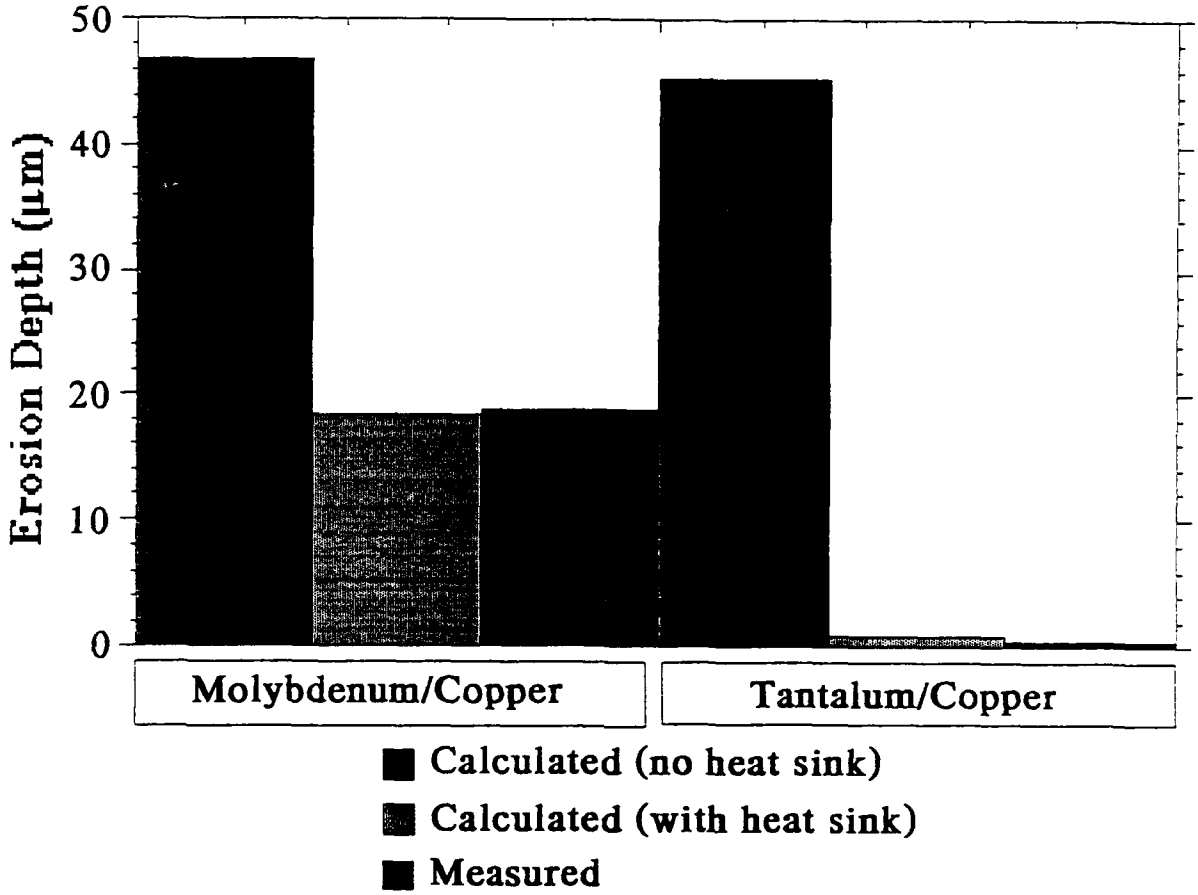

Calculated (with and without heat sink) and measured erosion depths of molybdenum and tantalum on copper substrates exposed to 33 GW/m^2 heat flux. Copper substrates have 6.35 mm diameter and 3.175 mm thickness. Molybdenum and tantalum coatings (prepared by sputtering) are, approximately, of 30 µm thickness. Calculated values are based on full energy deposition without vapor or melt shield.

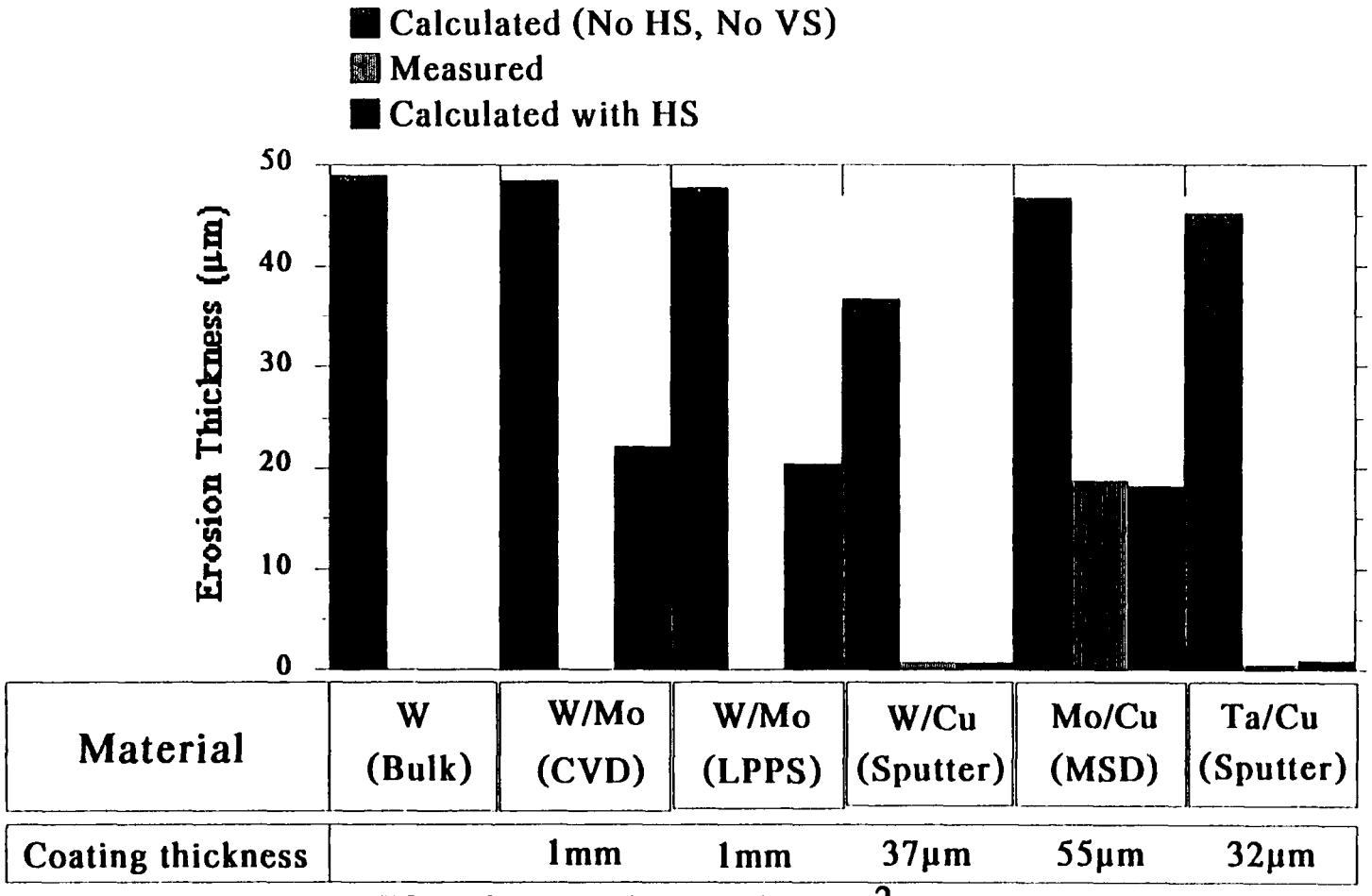

NCSU-SIRENS, 33 GW/m^2, 0.1 ms

Calculated and measured erosion of pure tungsten, tungsten coating on molybdenum and copper, and molybdenum and tantalum coating on copper. CVD = Chemical Vapor Deposition, LPPS = Low Pressure Plasma Spray, MSD = Molten Salt Deposition. HS and VS stand for Heat Sink and Vapor Shield, respectively.

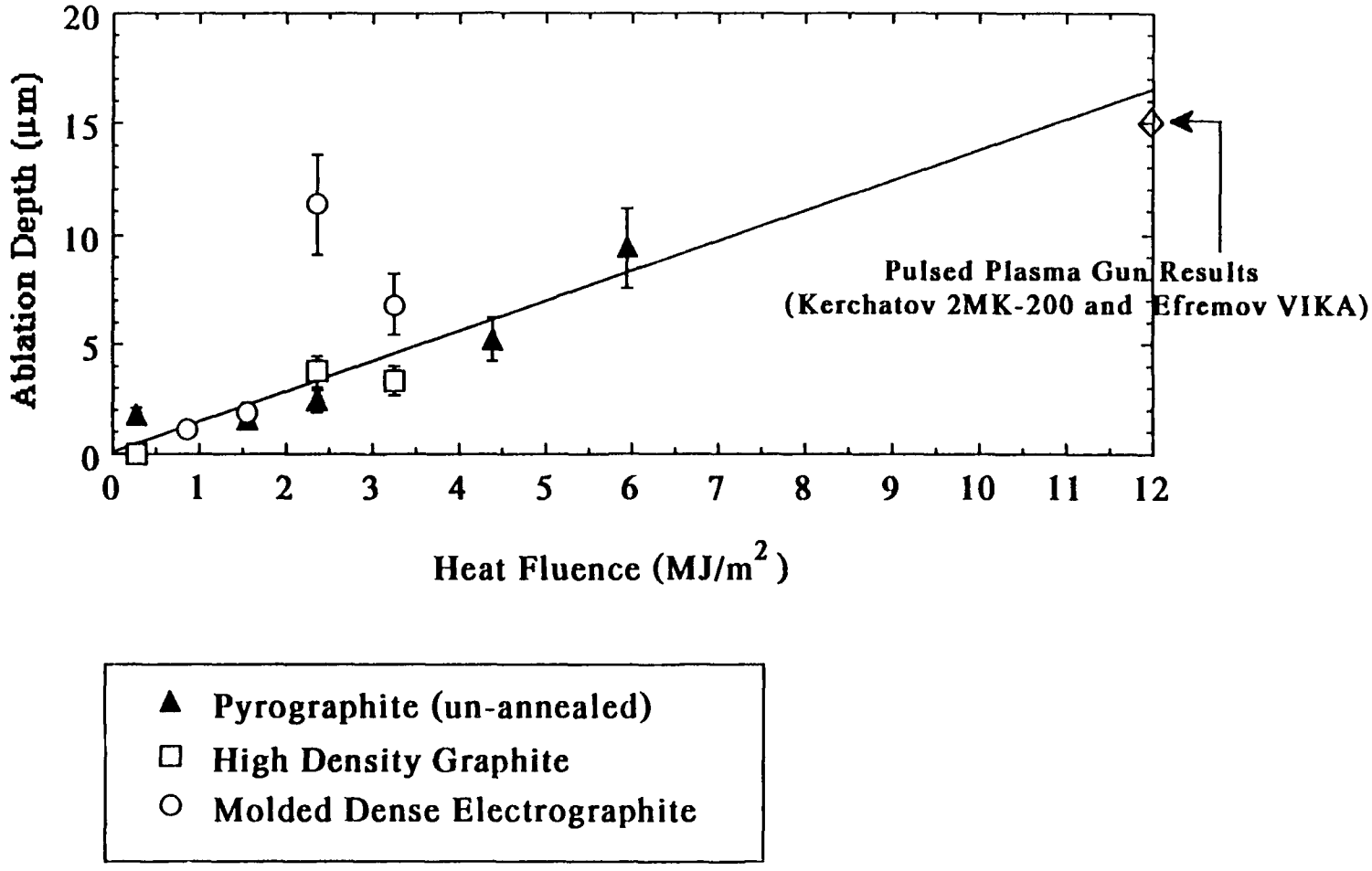

Measured graphite erosion as a function of incident heat fluence (SIRENS experiment).

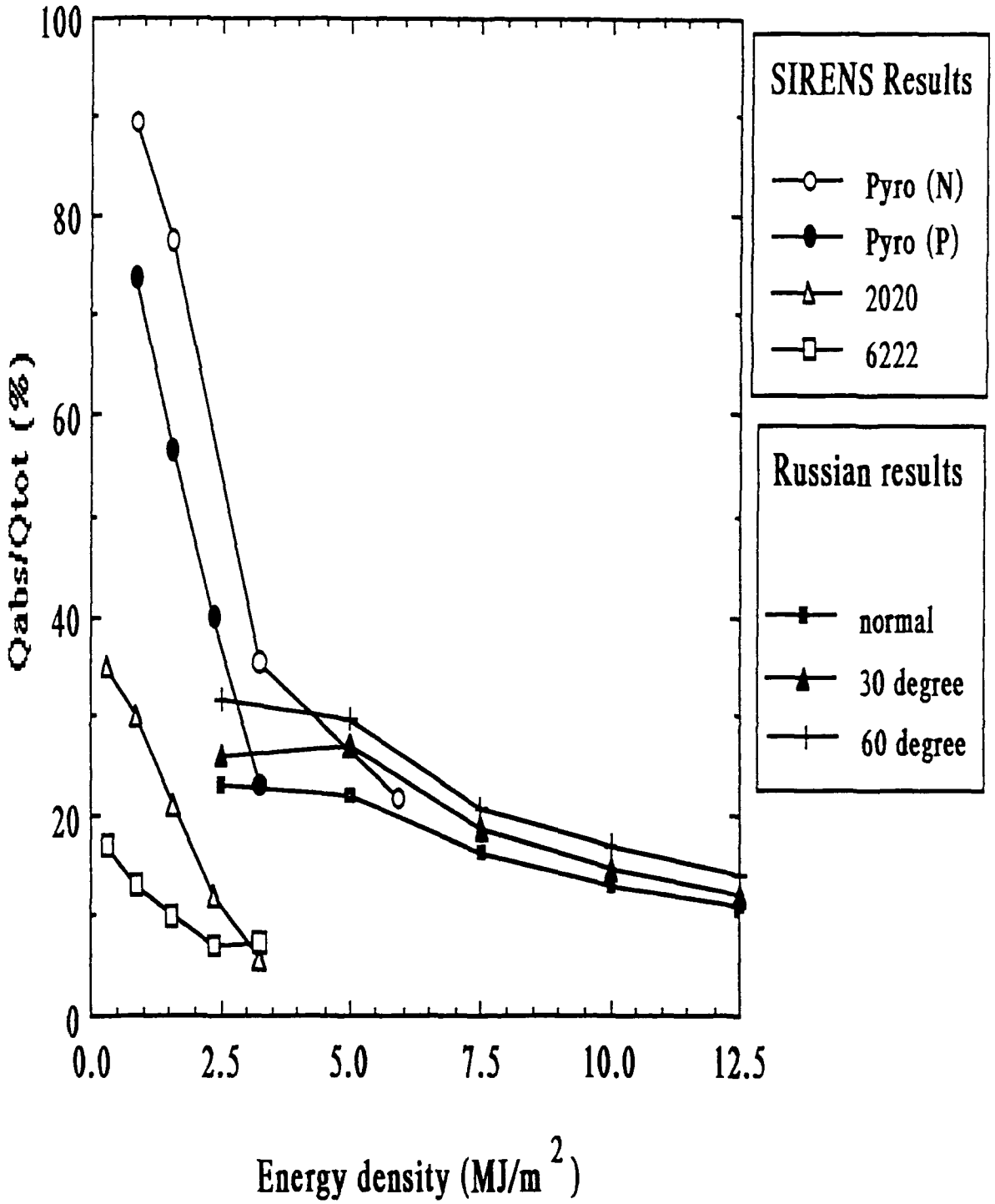

VAPOR SHIELD EFFECT

Comparison between SIRENS and Efrimov results on graphite

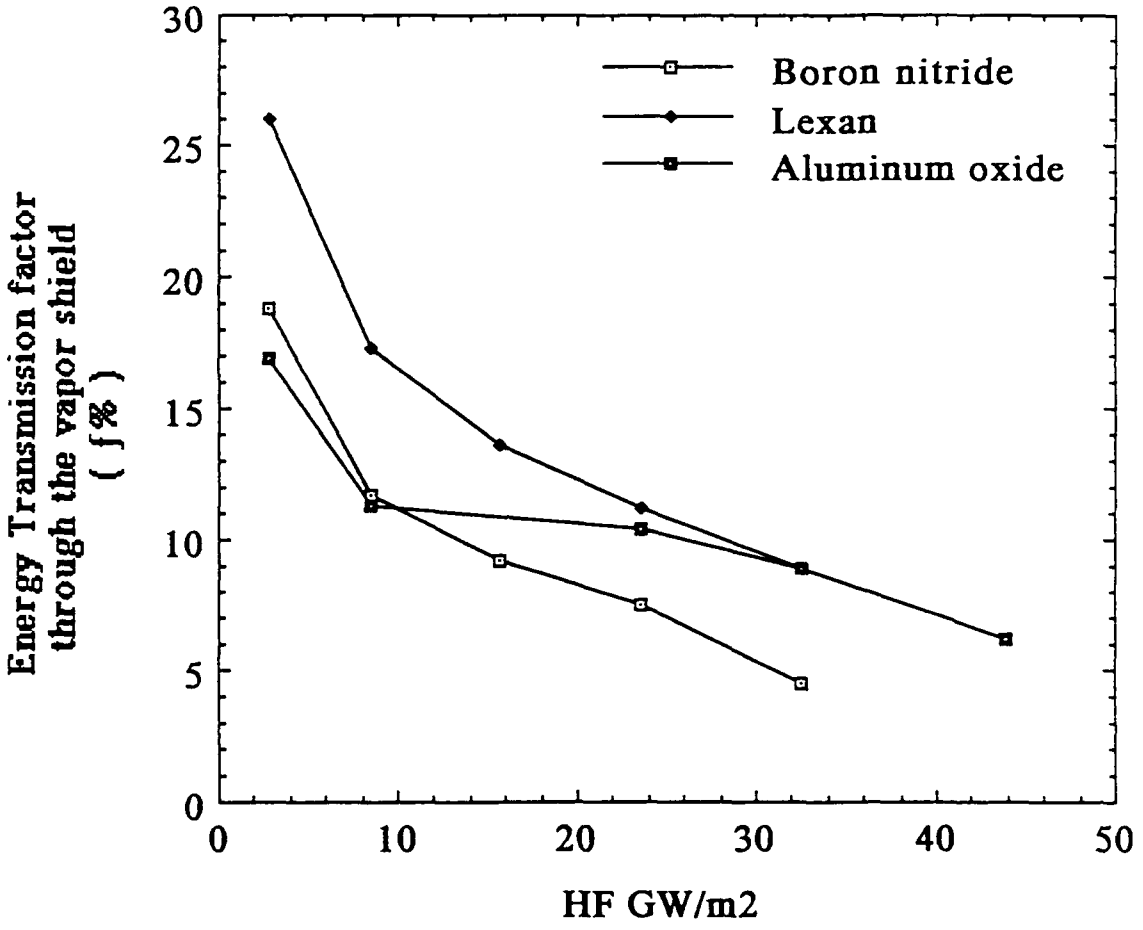

Energy transmission factor through the boundary layer "vapor shield" for three insulators of interest for EM, ET and ETC launchers

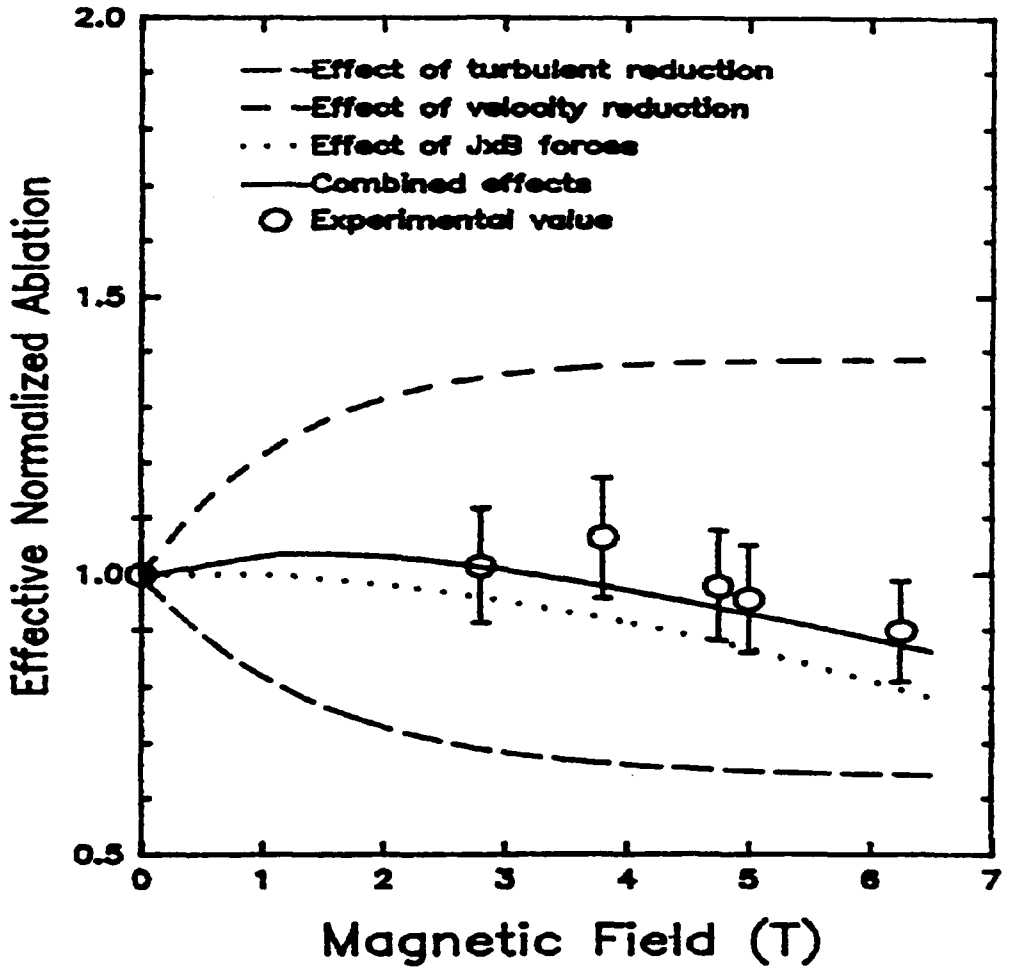

Individual and combined effects of plasma velocity slowdown, attenuated photon intensity and suppression of turbulence on surface ablation as functions of the externally applied parallel magnetic field, at an input energy of 3 kJ. The combined effect on ablation is in good agreement with the experimentally obtained normalized ablation.

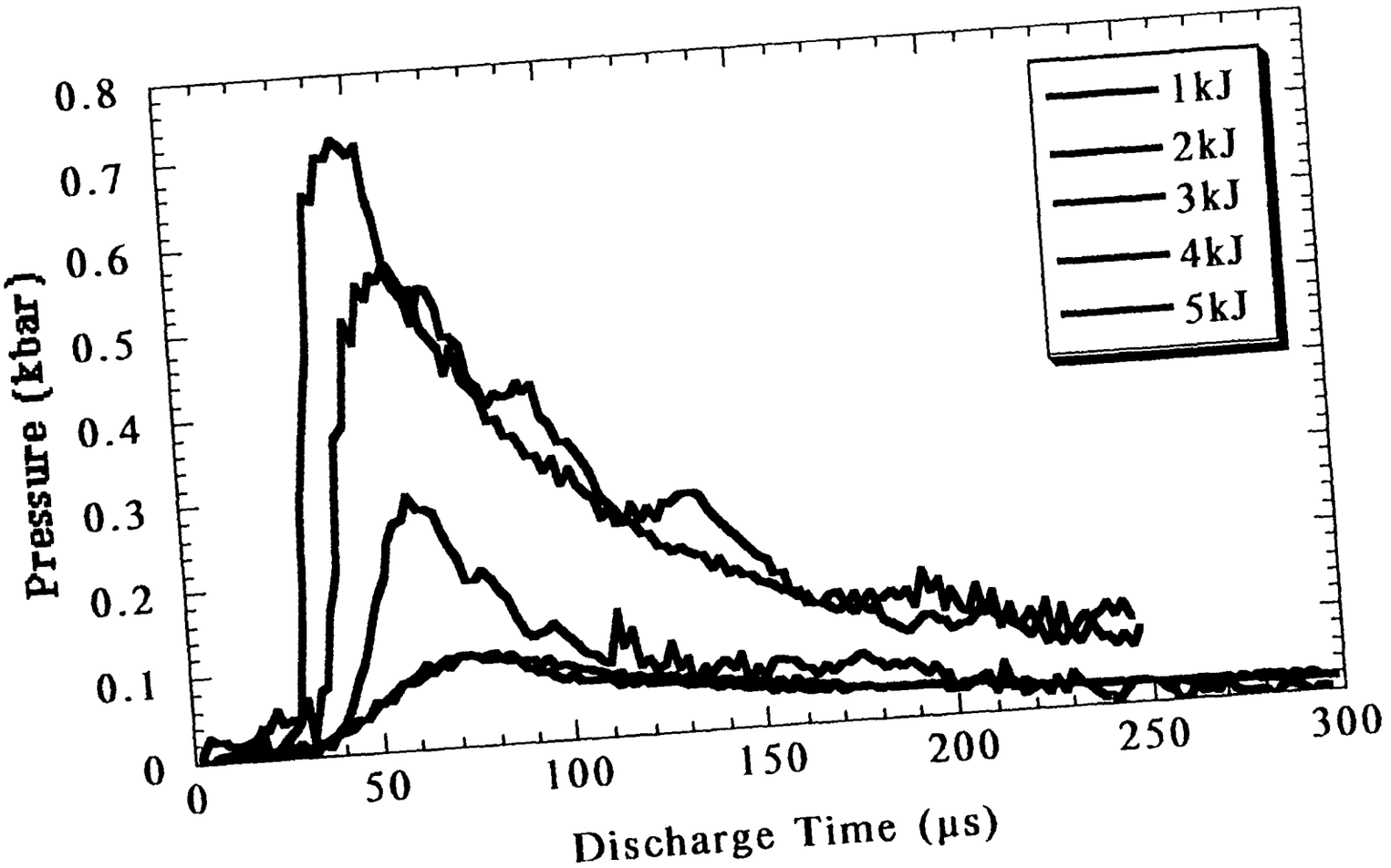

Absolute pressure measured inside the barrel, 2.5 cm from the breech, at different values of input energy. Fuseless operation with 2 Torr base pressure "air".

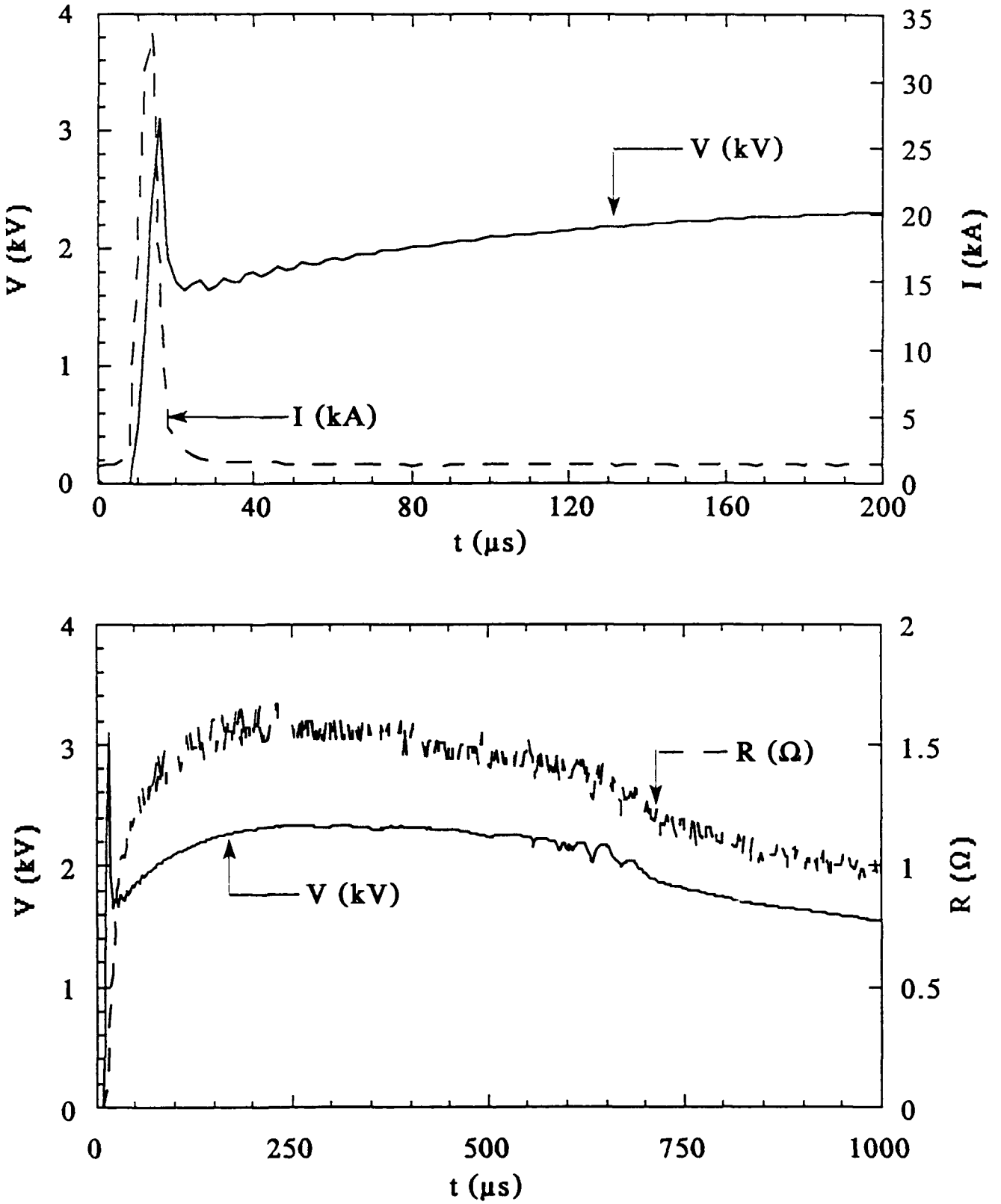

SHOT # 0489 FUSE OPERATION

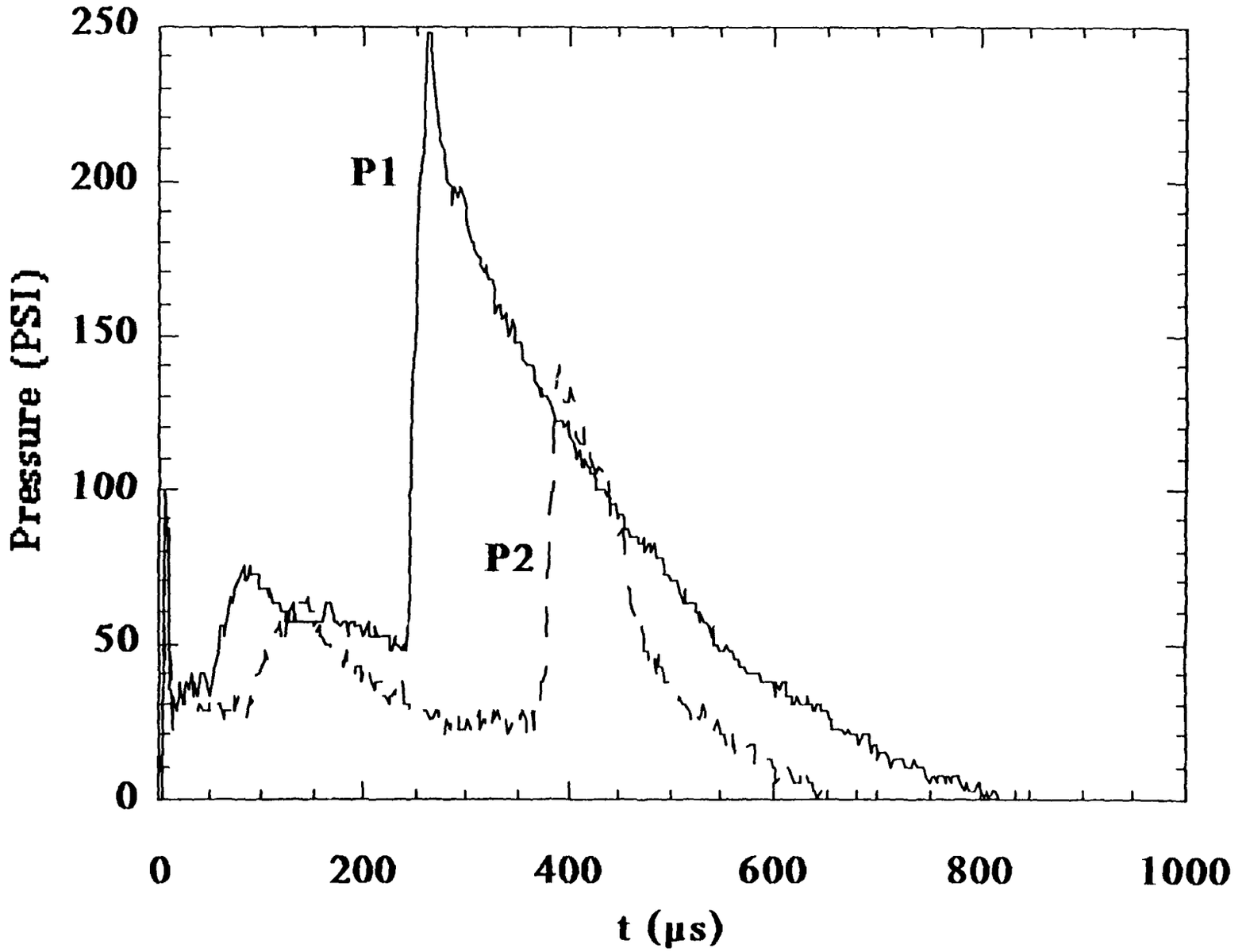

SHOT # 0489 FUSE OPERATION

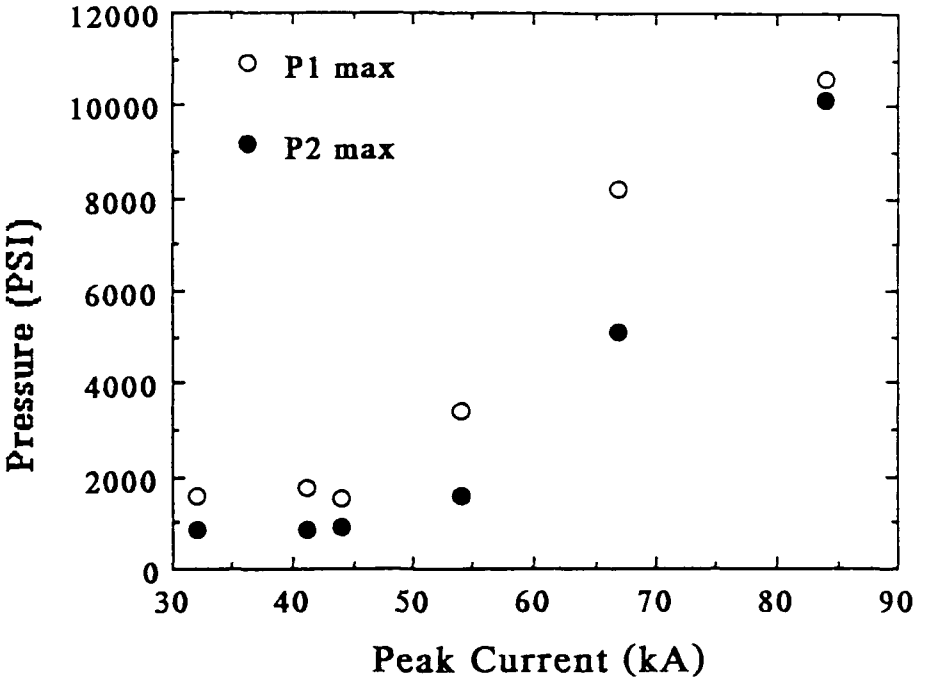

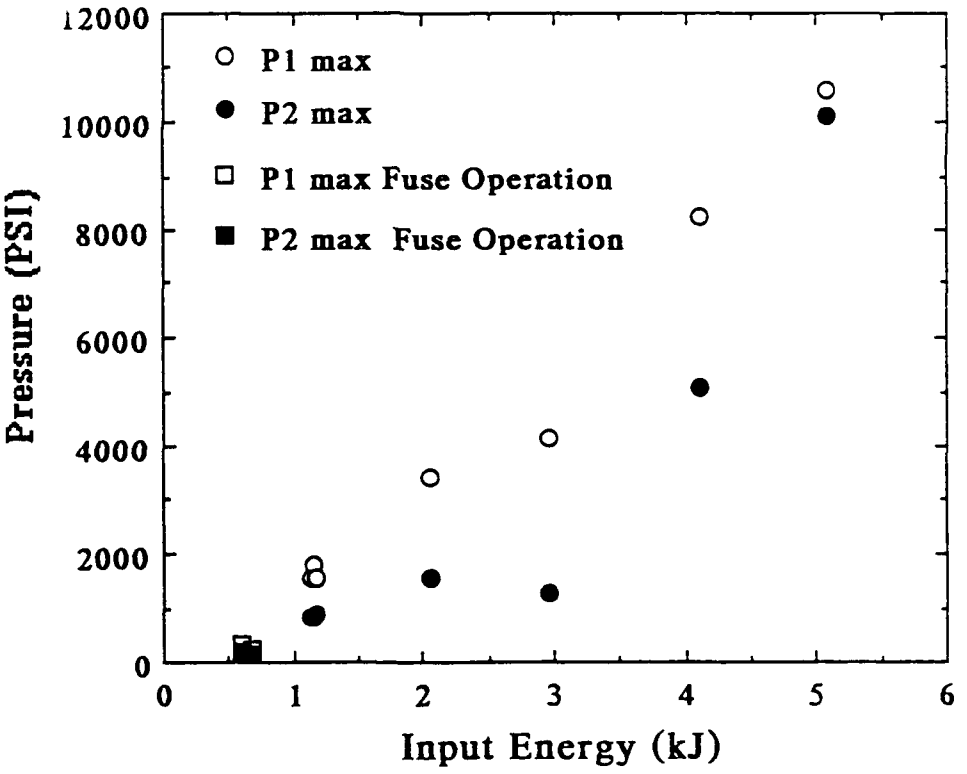

Peak pressures for fuseless (vacuum) and fuse operation (atmospheric)

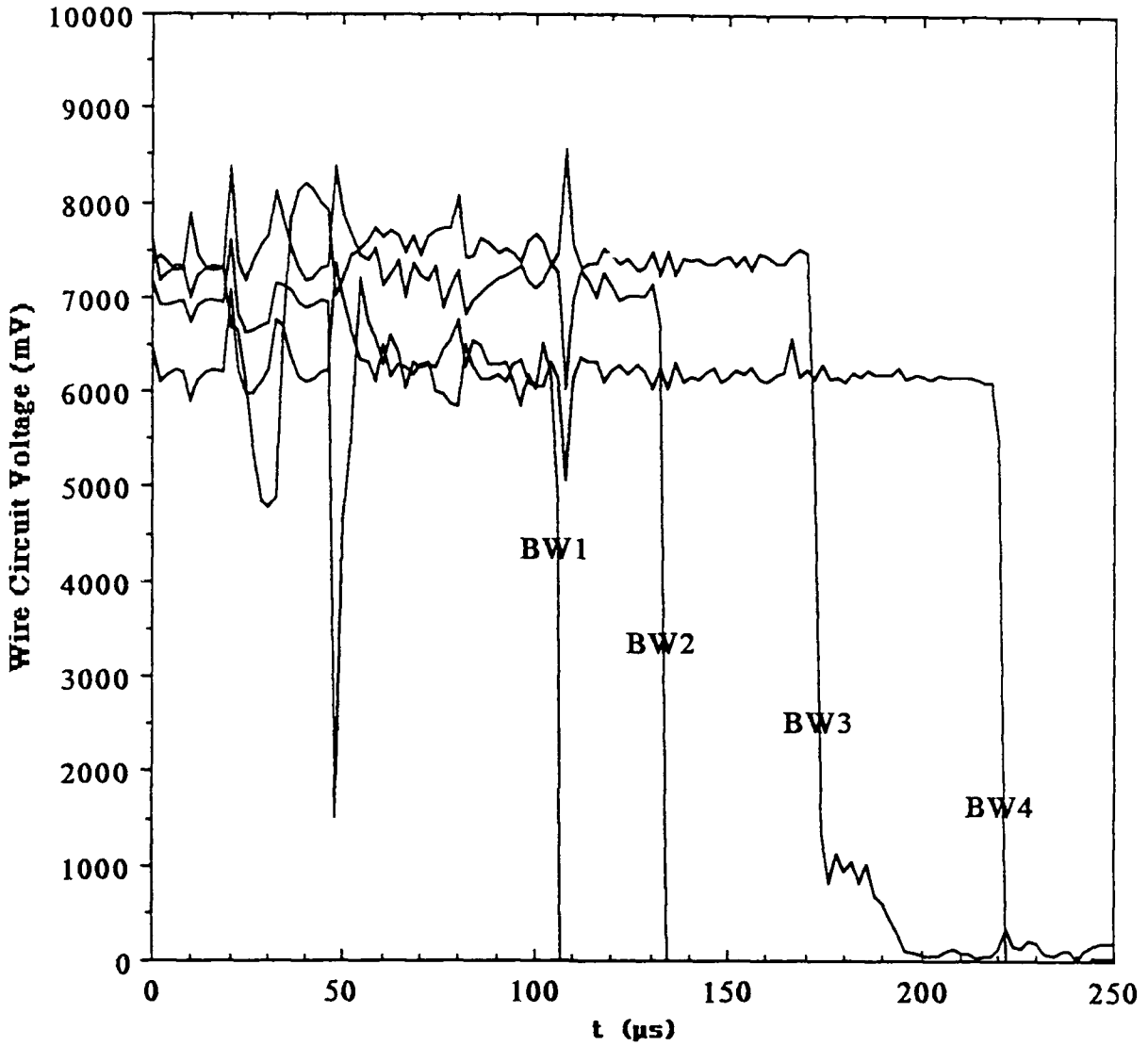

SHOT # 494
INPUT ENERGY 1.2 KJ
FUSE OPERATION "ATMOSPHERIC"
BREAK-WIRES TRACES

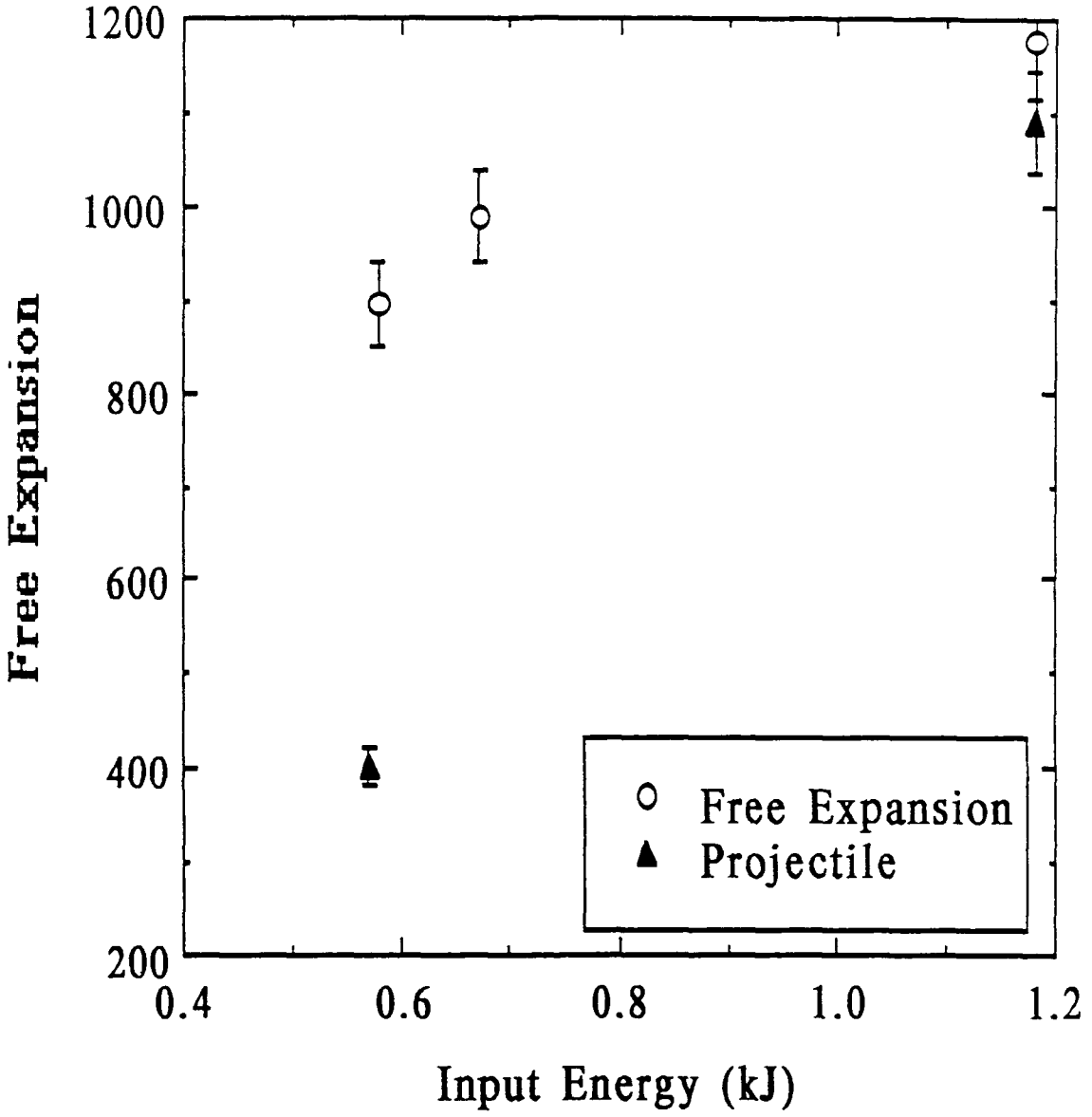

Fuse Operation (Atmospheric)
Projectile: 330 mg Lexan, 6 mm diameter

Shot # 0414, Sample # W220
Incident Heat Flux 33 GW/m^2

Unexposed sample, magnification 2000x

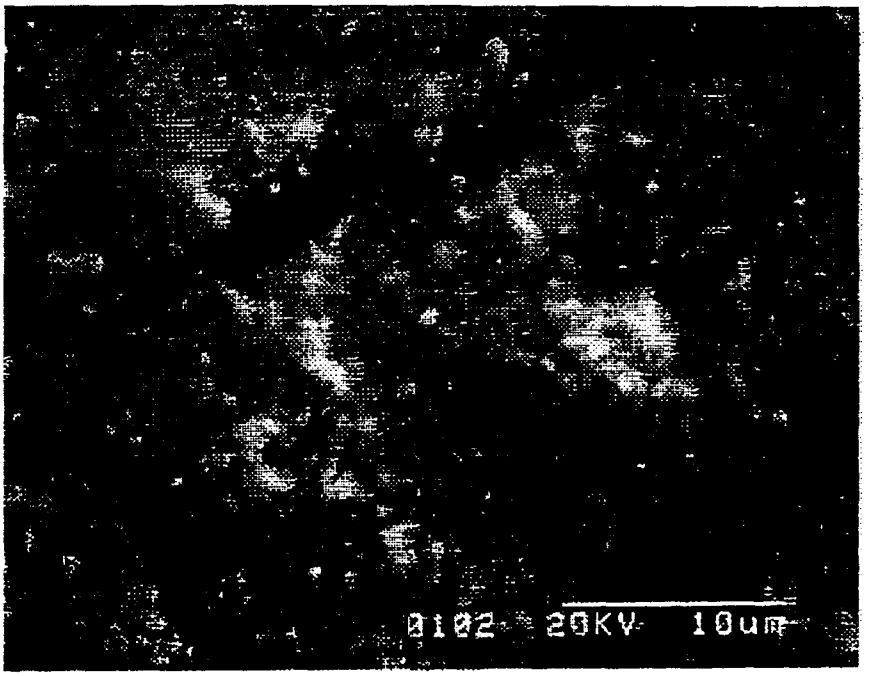

Exposed sample, magnification 3000x

SEM micrographs of unexposed (top) and exposed (bottom) diamond coating on a single crystal silicon wafer (10-13 μm diamond coating thickness on 25.4 mm diameter x 0.5 mm thick single crystal silicon wafer, coating processing parameters: 2% CH_4, 55 Torr, 300 scans, 26 hours).

Shot # 0415, Sample # W26
Incident Heat Flux 33 GW/m^2

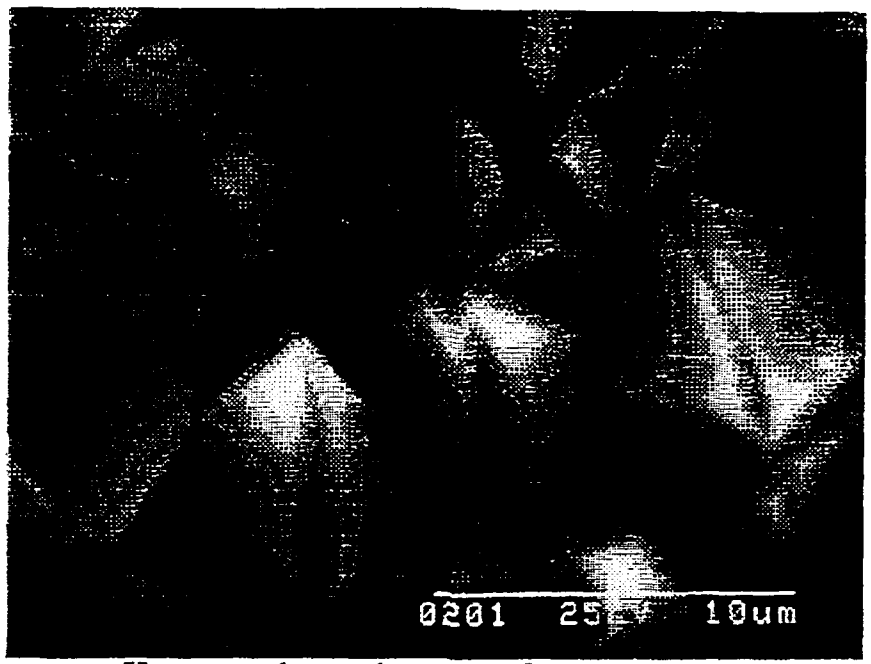

Unexposed sample, magnification 5000x

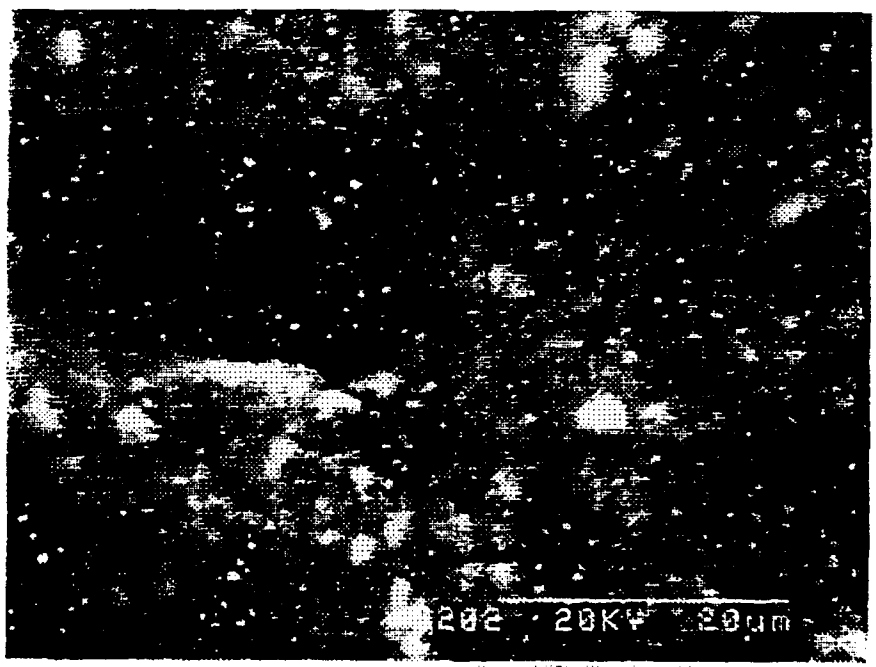

Exposed sample, magnification 2000x

SEM micrographs of unexposed (top) and exposed (bottom) diamond coating on a single crystal silicon wafer (10-13 µm diamond coating thickness on 25.4 mm diameter x 0.5 mm thick single crystal silicon wafer, coating processing parameters: 2% CH_4, 55 Torr, 300 scans, 26 hours).

Shot # 0464, Sample # PY1
Incident Heat Flux 4 GW/m^2

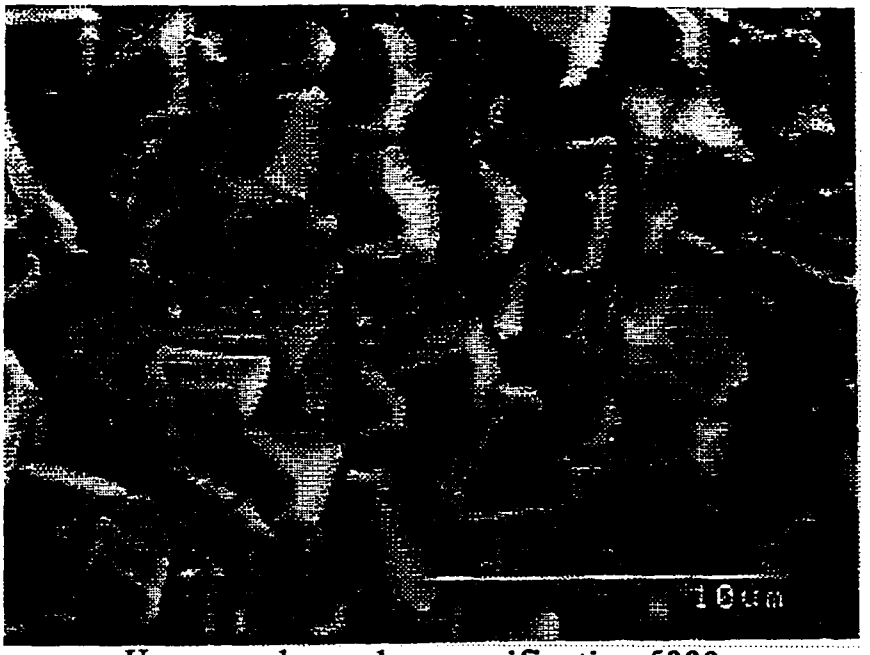

Unexposed sample, magnification 5000x

Exposed sample, center of impact, magnification 5000x

SEM micrographs of unexposed (top) and exposed (bottom) diamond coating on a single crystal silicon wafer (15 μm diamond coating thickness on 25.4 mm diameter x 3.3 mm thick single crystal silicon wafer, coating processing parameters: 2% CH_4, 55 Torr, 300 scans, 32 hours).

Shot # 0470, Sample # W-11N
Incident Heat Flux 3 GW/m^2

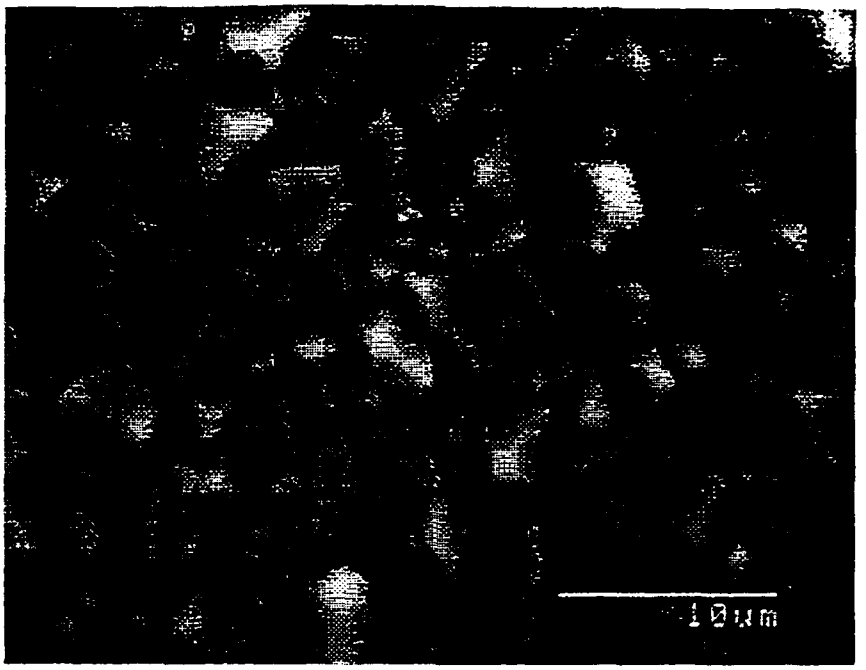

Unexposed sample, magnification 3000x

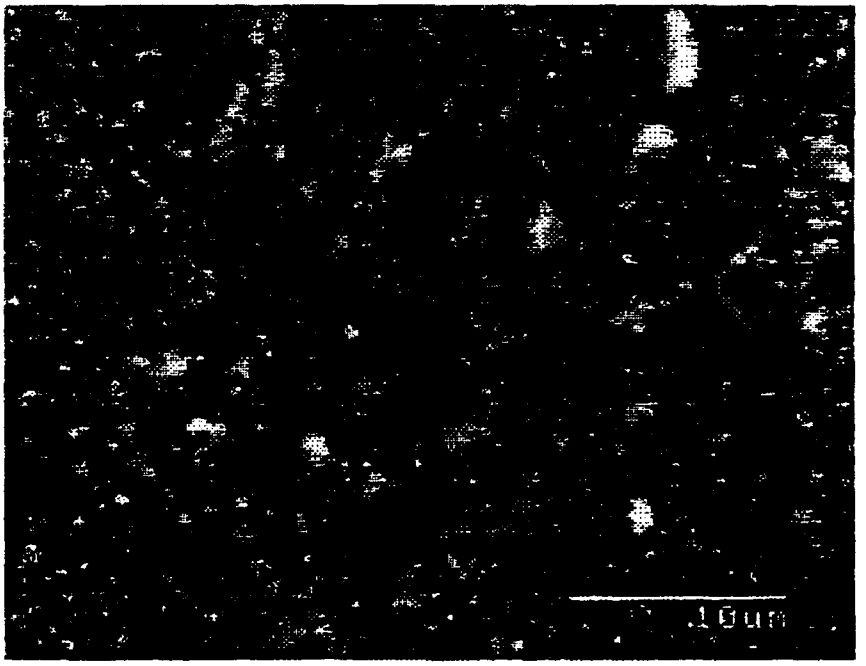

Exposed sample, magnification 3000x

SEM micrographs of unexposed (top) and exposed (bottom) diamond coating on a single crystal silicon wafer (20 µm diamond coating thickness on 25.4 mm diameter x 3.3 mm thick single crystal silicon wafer, coating processing parameters: 2% CH_4, 55 Torr, 300 scans, 36 hours).

Shot # 0471, Sample # W-12N
Incident Heat Flux 1 GW/m^2

Unexposed sample, magnification 3000x

Exposed sample, edge of impact, magnification 3000x

SEM micrographs of unexposed (top) and exposed (bottom) diamond coating on a single crystal silicon wafer (20 µm diamond coating thickness on 25.4 mm diameter x 3.3 mm thick single crystal silicon wafer, coating processing parameters: 2% CH_4, 55 Torr, 300 scans, 36 hours).

1993 PLANS

- Continuous materials erosion studies, potentially on full section of a railgun barrel.
- Acceleration studies using several projectile geometry and material, on fuseless "vacuum" and fuse "atmospheric" operation.
- Drag forces studies with and without a projectile.
- Development of new diagnostics for boundary layer and armature physics studies.
- Studies on plasma-propellant interactions "solid and liquid propellants" and energy transport process "propellant burn rates", and the flame vapor shield mechanism.
- Modeling and prediction of the flame vapor shield effect and burn rate of propellants.
- Detailed measurements and analysis of the magnetic vapor shield effect at higher values of magnetic fields, and higher heat fluxes.
- Ablation physics at surface "boundary layer" (1-D), includes heat transfer.
- Turbulent plasma boundary layer analysis (2-D), to explain magnetic field effects.

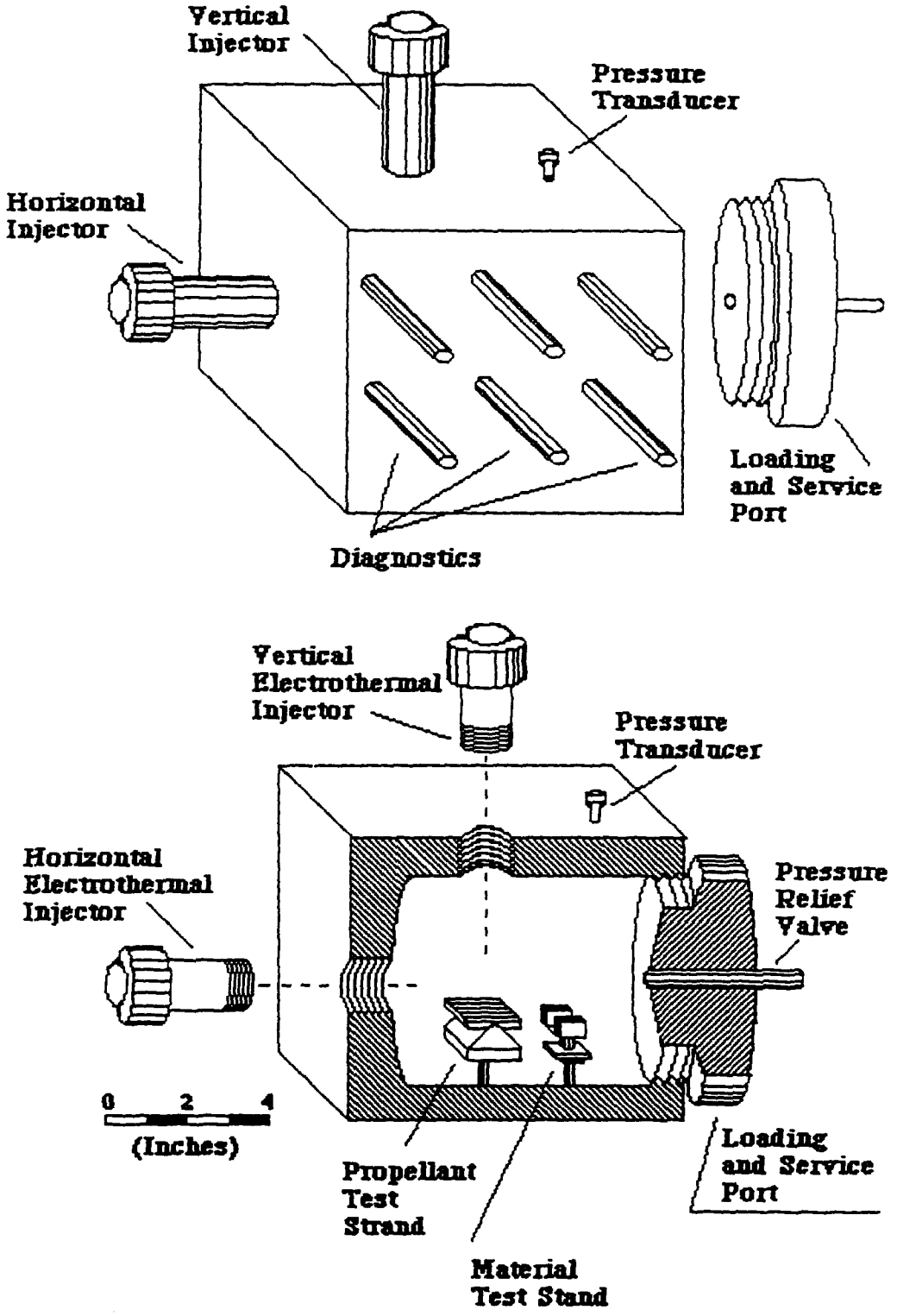

ISOMETRIC AND CUTAWAY VIEWS OF THE MODIFIED COMBUSTION CHAMBER, SHOWING DIAGNOSTICS ACCESS, PROPELLANT AND SAMPLE TEST STANDS (PIVOTING), AN ABSOLUTE PRESSURE TRANSDUCER FOR CHAMBER PRESSURE, AND THE LOADING AND SERVICES PORT WITH A PRESSURE RELIEF VALVE.

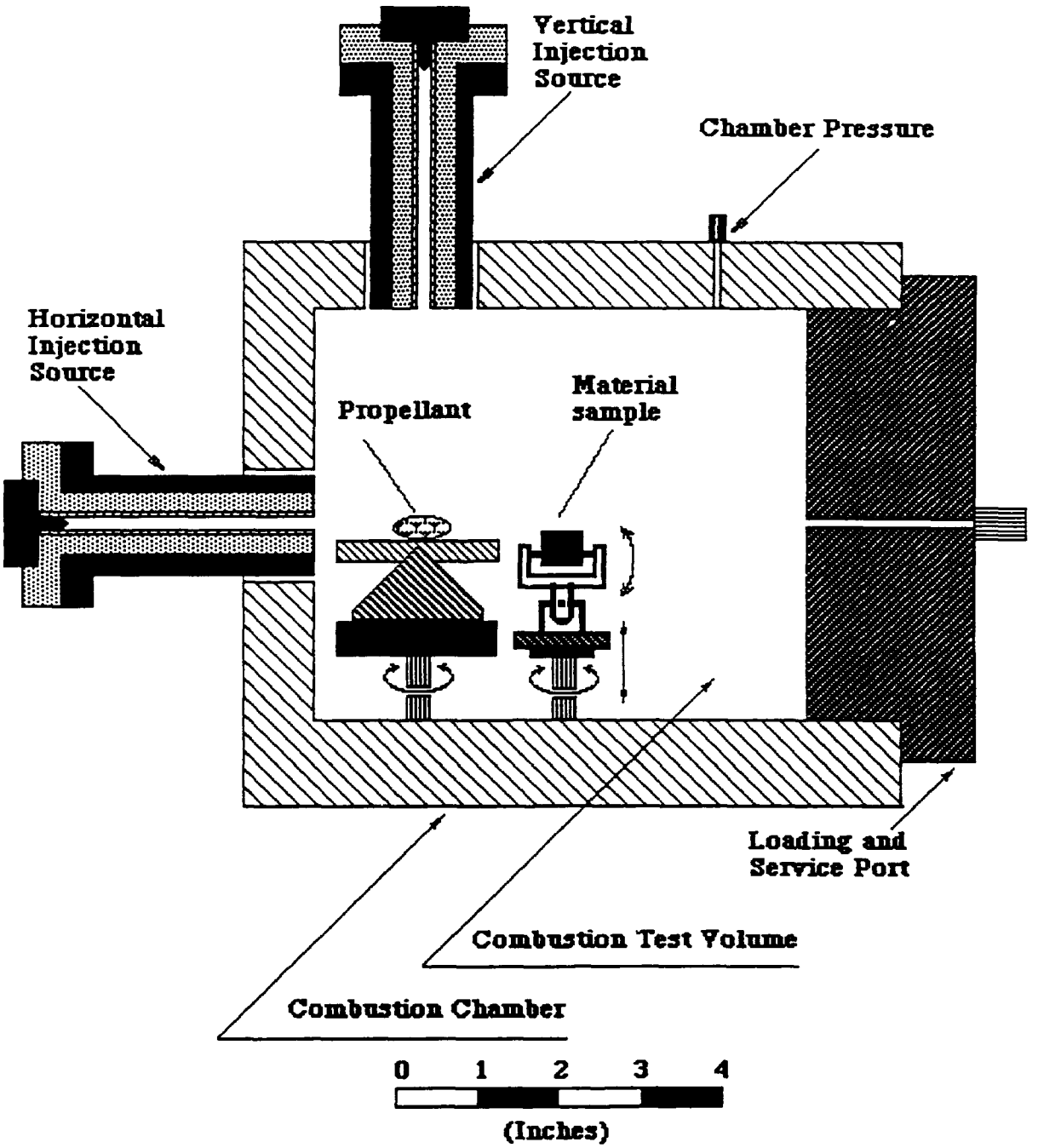

CONCEPTUAL DESIGN OF THE MODIFIED COMBUSTION CHAMBER. THE CHAMBER IS CUBICAL "6 INCH, 6-WAY STAINLESS STEEL CUBE" AND INCLUDES TWO 3-D POSITIONING PIVOT TEST STANDS FOR THE PROPELLANT AND THE MATERIAL SAMPLES.

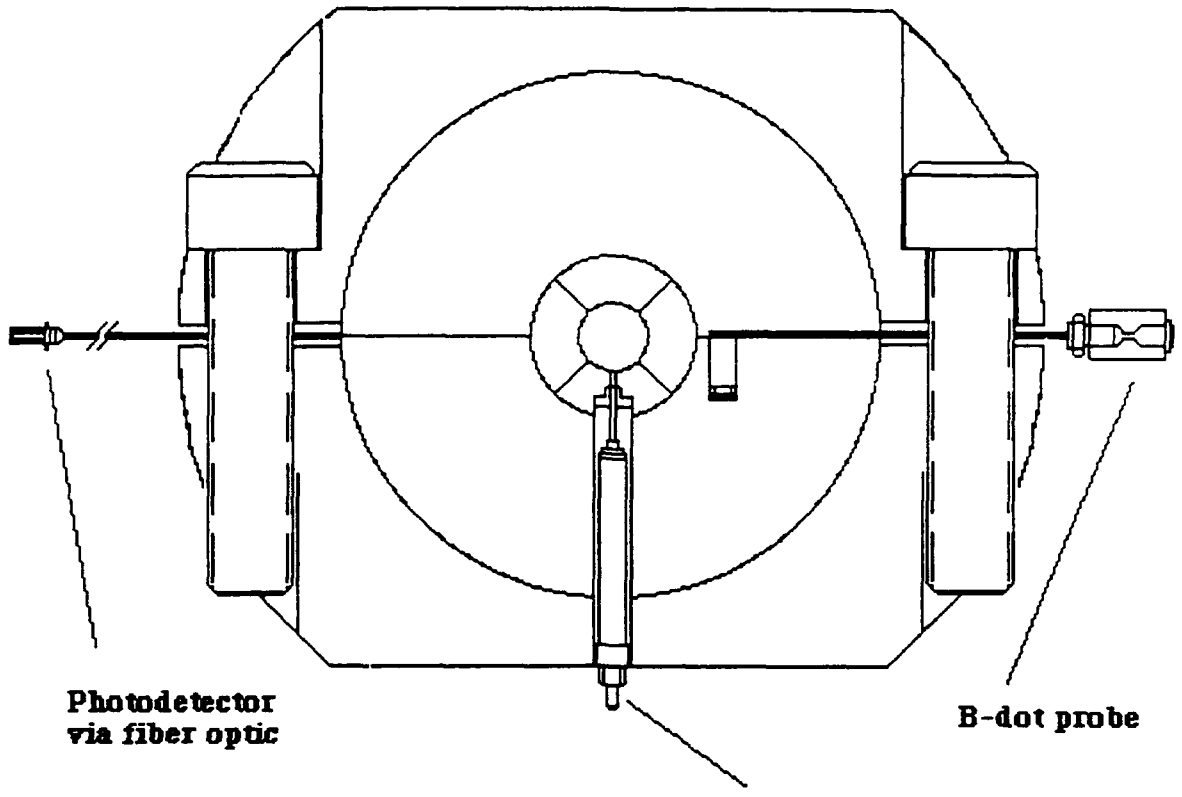
Photodetector
via fiber optic
B-dot probe
Absolute pressure
transducer

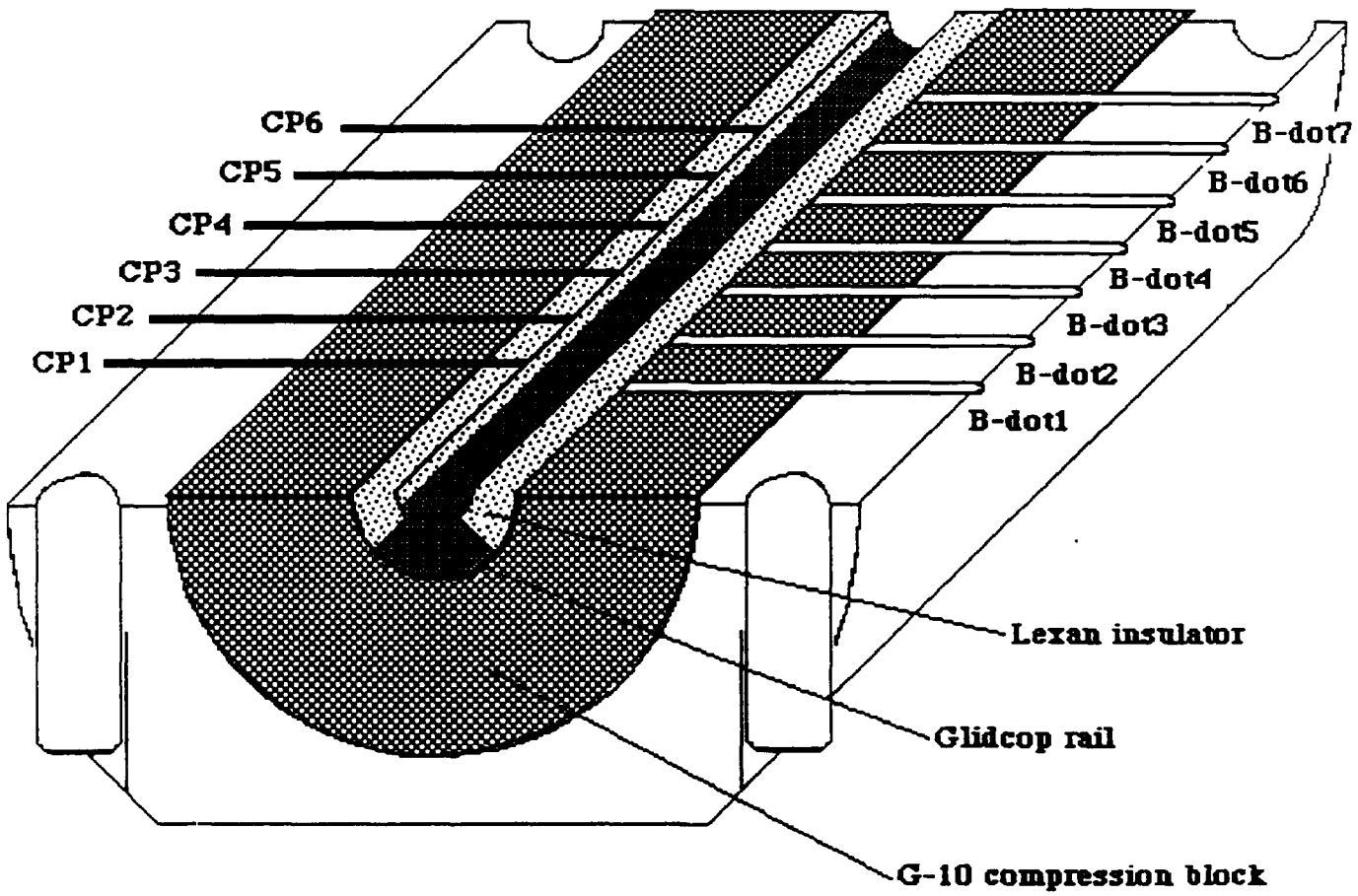
CP6
CP5
CP4
CP3
CP2
CP1
B-dot7
B-dot6
B-dot5
B-dot4
B-dot3
B-dot2
B-dot1
Lexan insulator
Glidcop rail
G-10 compression block

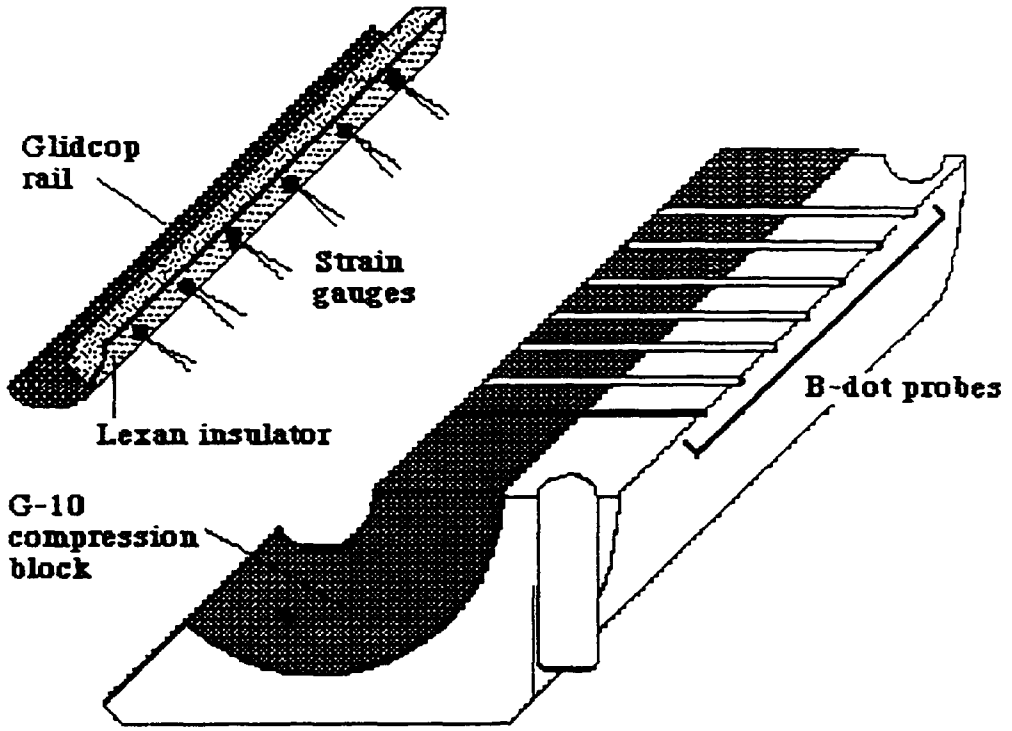

An isometric cutaway of the S0 railgun showing the strain gauges at locations between the insulator and the G-10 compressing block.

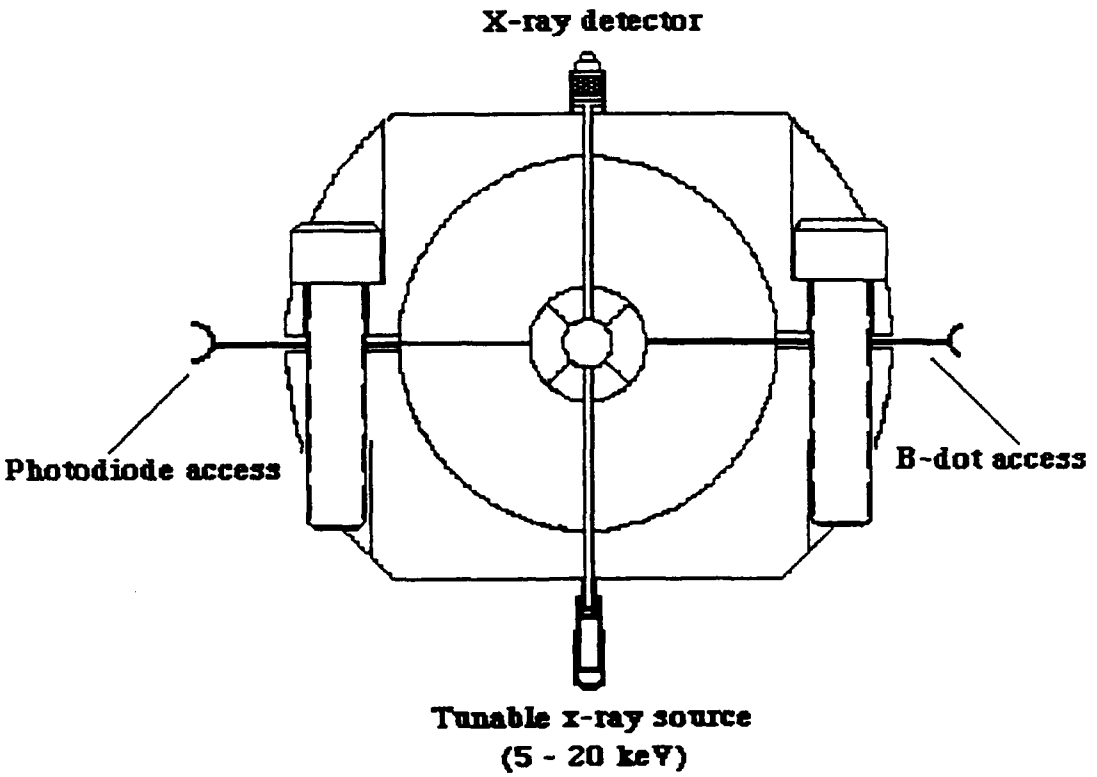

A schematic diagram showing the x-ray attenuation and scattering arrangement.